Chronic lung inflammation and CK14+ basal cell proliferation induce persistent alveolar-bronchiolization in SARS-CoV-2-infected hamsters

Can Li,[a,b,f] Na Xiao,[a,f] Wenchen Song,[a,f] Alvin Hiu-Chung Lam,[a,b,f] Feifei Liu,[a,f] Xinrui Cui,[e] Zhanhong Ye,[a,b] Yanxia Chen,[a,b] Peidi Ren,[e] Jianpiao Cai,[a] Andrew Chak-Yiu Lee,[a,b] Honglin Chen,[a,b] Zhihua Ou,[e] Jasper Fuk-Woo Chan,[a,b,c,d] Kwok-Yung Yuen,[a,b,c,d] Hin Chu,[a,b,d,**] and Anna Jin-Xia Zhang[a,b,*]

[a]State Key Laboratory of Emerging Infectious Diseases, Carol Yu Centre for Infection, Department of Microbiology, Li Ka Shing Faculty of Medicine, The University of Hong Kong, Pokfulam, Hong Kong SAR, China
[b]Centre for Virology, Vaccinology and Therapeutics, Hong Kong Science and Technology Park, Hong Kong SAR, China
[c]Department of Clinical Microbiology and Infection Control, The University of Hong Kong-Shenzhen Hospital, Shenzhen, China
[d]Department of Microbiology, Queen Mary Hospital, Pokfulam, Hong Kong SAR, China
[e]BGI Research, Beijing, China

eBioMedicine
2024;108: 105363
Published Online 25 September 2024
https://doi.org/10.1016/j.ebiom.2024.105363

Summary

Background Post-acute sequalae of COVID-19 defines a wide range of ongoing symptoms and conditions long after SARS-CoV-2 infection including respiratory diseases. The histopathological changes in the lung and underlying mechanism remain elusive.

Methods We investigated lung histopathological and transcriptional changes in SARS-CoV-2-infected male hamsters at 7, 14, 42, 84 and 120dpi, and compared with A (H1N1)pdm09 infection.

Findings We demonstrated viral residue, inflammatory and fibrotic changes in lung after SARS-CoV-2 but not H1N1 infection. The most prominent histopathological lesion was multifocal alveolar-bronchiolization observed in every SARS-CoV-2 infected hamster (31/31), from 42dpi to 120dpi. Proliferating (Ki67+) CK14+ basal cells accumulated in alveoli adjacent to bronchioles at 7dpi, where they proliferated and differentiated into SCGB1A+ club cell or Tubulin+ ciliated cells forming alveolar-bronchiolization foci. Molecularly, Notch pathway significantly upregulated with intensive Notch3 and Hes1 protein expression in alveolar-bronchiolization foci at 42 and 120dpi, suggesting Notch signaling involving the persistence of alveolar-bronchiolization. This is further demonstrated by spatial transcriptomic analysis. Intriguingly, significant upregulation of some cell-growth promoting pathways and genes such as *Tubb4b*, *Stxbp4*, *Grb14* and *Mlf1* were spatially overlapping with bronchiolization lesion.

Interpretation Incomplete resolution of SARS-CoV-2 infection in lung with viral residue, chronic inflammatory and fibrotic damage and alveolar-bronchiolization impaired respiratory function. Aberrant activation of CK14+ basal cells during tissue regeneration led to persistent alveolar-bronchiolization due to sustained Notch signaling. This study advances our understanding of respiratory PASC, sheds light on disease management and highlights the necessity for monitoring disease progression in people with respiratory PASC.

Funding Funding is listed in the Acknowledgements section.

Keywords: Hamster; PASC; Long COVID-19; SARS-CoV-2; Basal cell; Alveolar-bronchiolization

*Corresponding author. Department of Microbiology, Li Ka Shing Faculty of Medicine, The University of Hong Kong, Pokfulam, Hong Kong SAR, China.
**Corresponding author. Department of Microbiology, Li Ka Shing Faculty of Medicine, The University of Hong Kong, Pokfulam, Hong Kong SAR, China.
E-mail addresses: zhangajx@hku.hk (A.J.-X. Zhang), hinchu@hku.hk (H. Chu).
[f]These authors contribute equally to this study.

Research in context

Evidence before this study

We searched PubMed in May 2023, with no starting date limitations, using the terms "SARS-CoV-2" and "animal" and "basal cell" and "Long COVID" or "PASC" or "chronic" for articles in English. Our search identified a study that investigated CK14+ basal cell in hamster trachea up to 14 days-post-SARS-CoV-2-infection (dpi). Our search did not reveal any report systemically investigated the role of basal cell in lung regeneration and chronic histopathological changes long after SARS-CoV-2 infection in animals.

Added value of this study

In this study, we systemically investigated lung histopathological, transcriptional changes and dynamic activation, proliferation and differentiation of airway progenitor cell CK14+ basal cell during acute infection and lung regeneration including 7, 14, 42, 84 and 120 dpi in hamster, and compared with A (H1N1)pdm09 infection. We demonstrated persistent viral residues, chronic inflammatory and fibrotic changes from 42dpi to 120dpi. CK14+ basal cells activated and proliferated in bronchiolar epithelium at 7dpi. Meanwhile CK14+ basal cells migrated into alveoli, where they proliferated and differentiated into SCGB1A+ club cell or Tubulin+ ciliated cells, forming the lesion of alveolar-bronchiolization. Notch pathway was significantly upregulated. Intensive Notch3 and Hes1 protein expression were detected in alveolar-bronchiolization foci at 42, 84 and 120dpi, suggesting the association of sustained Notch signaling with persistence of alveolar-bronchiolization. This is further demonstrated by spatial transcriptomic analysis. Intriguingly, significant upregulation of some cell-growth promoting pathways and genes such as *Tubb4b*, *Stxbp4*, *Grb14* and *Mlf1* were spatially overlapping with bronchiolization lesion.

Implications of all the available evidence

Our data indicate incomplete resolution of SARS-CoV-2 acute infection in hamster lung with viral residue, chronic inflammatory and fibrotic tissue damage, and alveolar-bronchiolization, which may irreversibly impair the function of lung. Aberrant CK14+ basal cells proliferation and differentiation during tissue regeneration formed alveolar-bronchiolization persisted due to sustained Notch signaling. This study advances our understanding of respiratory PASC, sheds light on disease management and highlights the necessity for monitoring disease progression in people with respiratory PASC.

Introduction

Severe acute respiratory syndrome coronavirus 2 (SARS-CoV-2) caused more than 775 million infections and over 7.04 million deaths.[1] It is now known that about 10% of the COVID-19 patients recovered from SARS-CoV-2 infection experience a wide range of long-lasting symptoms and conditions which are defined as post-acute sequalae of COVID-19 (PASC) or long COVID.[2] Symptoms including dyspnea, chest pain, palpitations, nausea, abdominal pain, headache, fatigue, depression, anxiety and/or cognitive dysfunction last for more than 3 months or even longer after recovered from SARS-CoV-2 infection.[2,3] Among these, respiratory symptoms are reported in 5–40% of the patients with PASC[2,3]; dyspnea and persistent cough were reported in 40% and 20% of patients after 4–8 months, respectively.[2,3] A thoracic computed-tomography study reported 79.4% of 166 hospital-discharged patients had residual lung abnormalities after 8 months.[4] CT scans indicated fibrosis features in lung, including ground-glass opacification and reticulation.[4–6]

Current hypothesis of the mechanisms underlying the chronic pulmonary abnormalities includes viral persistence, tissue fibrosis, and dysregulated lung regeneration.[7,8] Viral persistence induces inflammation and possible fibrosis. Incomplete or prolonged alveoli and airway regeneration will lead to impaired capacity of gas exchange. It's crucial to elucidate lung regeneration process after SARS-CoV-2 infection which causes diffuse alveolar damage (DAD) with massive alveolar type (AT)1 and AT2 cell death.[9] Under this condition, multiple pulmonary progenitor cells could be activated for tissue repair along the resolution of acute inflammation.[10] AT2 cell itself has the potential multiply for self-renewal for tissue homeostasis and may also trans-differentiate into AT1 cells upon tissue injury.[11] When tissue injury is severe and involving AT2 cell death or depletion, multiple types of lung progenitor cells, including airway basal cells, club cells, bronchioalveolar stem cells (BASCs)[9–13] are activated to for tissue repair. Studies on bleomycin/LPS induced lung damage and influenza virus infection in mice had demonstrated the important roles of basal cells proliferation and differentiation in lung regeneration.[14–17] SARS-CoV-2 infection of human bronchial organoids showed that basal cells were relatively resistant to SARS-CoV-2 comparing to susceptible cell type such as ciliated cell; basal cells quickly responded to virus induced epithelial cell death by activation and differentiation.[18] CK5+ basal cells were reported to actively proliferate for alveolar repair in mice and human in influenza A and SARS-CoV-2 infection.[12,19] For progenitor cells to function properly in lung tissue repair, tightly regulated cell activation, proliferation and differentiation are prerequisites. Dysregulation of basal cell differentiation has been found to be associated with chronic obstructive pulmonary diseases (COPD) and pre-neoplastic lesions.[20,21] However, the role of basal cells in alveolar regeneration and lung

abnormalities after SARS2-CoV-2 infection has not been fully elucidated. Sparse or very limited availability of serial human lung samples hinders our understanding of the histopathology and molecular events in the lung of long COVID. To this end, we choose a previously established Golden Syrian hamster model, as it has been wildly accepted as a physiological relevant small animal model that simulated well human manifestations of acute SARS-CoV-2 infection.[22] This model is also considered superior to K-18 hACE2 mouse and ferret for studying SARS-CoV-2 infection related long-term sequelae[22–24] owning to its non-lethal nature of infection. Through studying serial lung tissue sections taken from SARS-CoV-2 infected hamsters, we demonstrated persistent viral residues, chronic inflammatory and fibrotic changes in the lungs long after acute infection. We further proved that it is CK14+ basal cells in distal airways which were activated and participated for bronchioles epithelium regeneration; however, CK14+ basal cells in alveoli continued to proliferate and differentiate to club cells and ciliated cells, forming multiple abnormal bronchiolization foci. The underlying molecular mechanism for the persistent bronchiolization is attributed, at least partly, to sustained activity of Notch signaling. We concluded that chronic inflammatory and fibrotic changes together with persistent alveolar-bronchiolization could be correlated to the long-lasting respiratory manifestation in human, while further investigations and long-term surveillance for disease progression are needed.

Methods

Virus, cell lines and biosafety

SARS-CoV-2 wild-type strain HK-13 (GenBank accession no. MT835140), and BA.5 strain (GISAID accession number: EPI_ISL_13777658) were isolated from laboratory-confirmed COVID-19 patients, propagated and titrated in African green monkey kidney cells overexpressing TMPRSS2 protein (Vero E6-TMPRSS2).[25] Human influenza virus A (H1N1)pdm09 (A/HK/415742/2009) mouse adapted strain, which can infect and cause pneumonia in hamster,[25] was chosen as control. A (H1N1)pdm09 mouse adapted virus was propagated in hen eggs and titrated in Madin–Darby canine kidney cells (MDCK).[25,26] Experiments involving infectious SARS-CoV-2 were performed following the approved standard operating procedures of the Biosafety Level 3 facility.

Animals

Male Golden Syrian hamsters, 6–8 weeks old with an average body weight of 105 ± 8 gram, were obtained from the Centre for Comparative Medicine Research, HKU. Animals used in this study were listed in Table S1. Sample size for animal number in each group was calculated by power analysis,[27] referenced on published similar study[28] and our own publication.[25] All the animal experimental procedures were approved by the Committee on the Use of Live Animals in Teaching and Research of HKU (CULATR #5783-21 and 6093-22) and the Institutional Review Board of Beijing Genomics Institute, Shenzhen, China (BGI-IRB A21031-T2).

Virus challenge in hamsters

Hamsters were randomly grouped and inoculated intranasally with 10^3 PFU SARS-CoV-2 or 10^5 PFU mouse-adapted A (H1N1)pdm09 virus in 50 μl volume per animal under anesthesia of ketamine (150 mg/kg) and xylazine (10 mg/kg) as we previously reported.[25] Mock-infection controls were given the same volume of PBS. At 4, 7, 14, 42, 84 or 120dpi, hamsters were euthanized by intraperitoneal injection of pentobarbital sodium (200 mg/kg). Blood and lung tissues were harvested for analysis.

RNA extraction and RT–qPCR

Total RNA extracted from homogenized lung tissues was reverse transcribed into cDNA using MiniBEST Universal RNA Extraction Kit (Takara) and PrimeScript™ RT reagent kit (Takara). RT-qPCR was performed using QuantiNova Probe PCR Kit (Qiagen) or SYBR Premix Ex Taq II Kit (Takara) with gene-specific primers (Table S2). The expression of cytokine/chemokine and Notch signaling pathway/Fibrosis related genes was analyzed by ΔΔCt method, using mock control animals with similar age as baseline.

Histopathology, immunohistochemistry and immunofluorescence staining

Formalin-fixed, paraffin-embedded lung tissues were processed into 4 μm sections and stained with hematoxylin and eosin (H&E) for histopathological examination. Viral antigens and cellular proteins were detected by immunohistochemistry or immunofluorescence with specific antibodies: home-made rabbit/mouse anti-SARS-CoV-2 nucleocapsid protein antibody,[25] home-made mouse anti-H1N1 nucleocapsid protein antibody,[25] anti-Ki67 antibody (556003, BD; ab15580, Abcam), anti-β tubulin-IV antibody (T7941, Sigma), anti-CK14 antibody (PA516722, Invitrogen; MA5-11599, Invitrogen), anti-SCGB1A1 antibody (10490, Proteintec), anti-SPC antibody (ab3786, Millipore), anti-Iba1 antibody (ab178846, Abcam), anti-Notch3 antibody (MBS242006, MyBioSource), anti-Hes1 antibody (LS-B2211 LSBio), anti-Sox2 antibody (11064-1-AP, Proteintech) and anti-Mlf1 antibody (MBS9605647, MyBioSource). Fibrosis staining was performed using NovaUltra Massion Trichrome Stain Kit (IW3006, IHC World) according to the manufacturer's instructions.

Digital image analysis

All tissue sections were examined under light or fluorescence microscopy in a blind fashion. Whole slide

images were captured with Akoya Vectra Polaris Scanner at 200× magnification (Akoya Bioscience, USA). Sectional images were captured by Olympus BX53 Light Microscope (Olympus Life Science, USA). Confocal images were captured with Zeiss LSM900 with AiryScan 2 with 40× and 63× oil objectives. Bronchiolization foci were annotated with QuPath using whole slide scanned images and semi-quantification scoring was manually performed (Fig. S6). The severity of collagen deposition was examined with Masson Trichrome stained lung sections and scored using the modified Ashcroft scale as described.[29] For quantification of specific cell marker positive cells, randomly captured images of immunofluorescence-stained lung sections in the whole lung of examined hamsters were analyzed with QuPath (Version 0.4.4).

Bulk RNA-seq experiment and data analysis

Total RNA from lung tissue cells for hamsters was isolated using NucleoSpin RNA Kit (740955.250, Macherey–Nagel, Duren, Germany). cDNA libraries were prepared by KAPA mRNA HyperPrep Kit following the standard protocol. The libraries were denatured and diluted to optimal concentration. Illumina NovaSeq 6000 was used for Pair-End 151bp sequencing. Raw sequencing data were filtered with fastp v0.20.1 to remove adapters and low-quality reads. The alignment file was used for assembling transcripts, estimating their abundances, and detecting differential expression of genes. The genes expression level was quantified by HISAT2 v2.2.0[30] (Reference genome: BCM_Maur_2.0 & grcm38/release_M25). Principal components analysis (PCA) was conducted in R v4.0. Differentially expressed genes were determined based on counts using DESeq2 v3.15[31] based on the following thresholds: |log2FC|>1 and FDR value < 0.05. Metascape[32] was used to conduct functional enrichment analysis involving Gene Ontology (GO) and the Kyoto Encyclopedia of Genes and Genomes Pathway (KEGG) for the DEGs with p-value<0.05. The reference species was *Mesocricetus auratus*.

Spatial transcriptomics experiment and analysis

Formalin-fixed, paraffin-embedding (FFPE) lung tissues were collected for Stereo-seq experiment. Library preparation was performed using the Stereo-seq FFPE Transcriptome Kit and Stereo-seq 16 Barcode Library Kit V1.0 (STOmics Tech, China) according to the manufacturer's protocol. The Stereo-seq chip was 1cm × 1 cm in size, which contained capture spots with a diameter of 220 nm and a spot-to-spot distance of 500 nm.[33] The capture probes contained random primers to capture RNAs. In brief, 5 μm FFPE lung tissue section was cut, fully spread, and placed on the Stereo-seq chip. One adjacent tissue section was cut for H&E staining. After dewaxing and decrosslinking reaction, the tissue section was permeabilized to release RNA for in situ hybridization. After RNA capture, reverse transcription was performed, and cDNA was later released. The cDNA was then purified and amplified with PCR mix. The PCR products were used to prepare library, which was sequenced by an MGI DNBSEQ T series sequencer (MGI-TECH, China). The spatial transcriptomic data was analyzed with a unit of bin100 (49.72 μm × 49.72 μm). Raw sequencing data were processed using the SAW pipeline (https://github.com/BGIResearch/SAW). High-quality reads were annotated to generate the spatial gene expression matrix by SAW process V6.1 and handleBam.[34] Seurat (v4.9.9) was used for further quality control, SCT normalization, dimensionality reduction, clustering, principal component analysis and identification of gene expression patterns.[35] Technically, functional gene enrichment analysis was performed with clusterProfiler, and the DEGs between the abnormal and normal regions were identified with adjusted p-value <0.05.

Statistical analysis

All data were analyzed with Prism 8.0 (GraphPad Software Inc). Data were checked for normal distribution using Shapiro–Wilk test and Kolmogorov–Smirnov test. Statistical comparison among different groups were performed using One-way ANOVA with Tukey's multiple comparisons test, Two-way ANOVA with Tukey's multiple comparisons test, or Kruskal–Wallis test with Dunn's multiple comparisons test. $p < 0.05$ was considered statistically significant.

Role of funders

Funders had no role in study design, data collection, data analyses, interpretation, or writing of report.

Results

Prominent chronic histopathological damages found in the lung of hamster recovered from SARS-CoV-2 infection

To characterize the temporal histopathological changes in lung after SARS-CoV-2 infection, we conducted a longitudinal study using 6–8 weeks old hamsters challenged with 10^3 PFU of SARS-CoV-2 wild-type strain HK-13 and observed till 120dpi (Fig. 1a). The most prominent histological feature of the lung at 120dpi was multiple foci of alveolar hyperplasia (Fig. 1b). The lung structure showed alveolar consolidation with increased thickness of alveolar septa while reduced and collapsed air sac; peribronchiolar and perivascular immune cell infiltration were also commonly observed in almost every lung lobe (four lobes were examined for each animal) (Fig. 1b). Pleural fibrosis showed in H&E-stained section was also observed in half of the infected hamsters (6/12) (Fig. 1b). The alveolar hyperplasia foci were readily seen in all the examined lungs (12/12) under a 4 × microscope, which distributed from

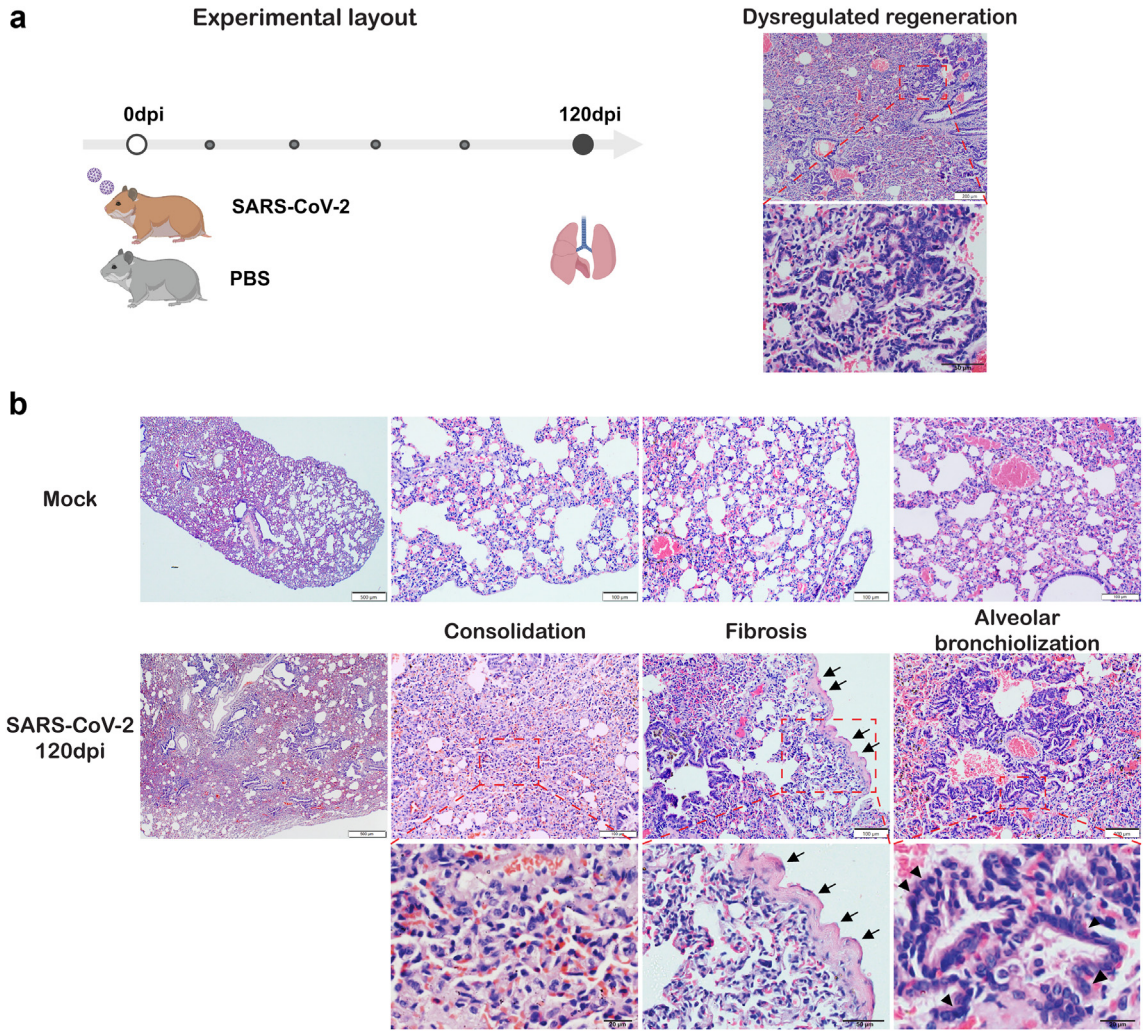

***Fig. 1:* SARS-CoV-2 infection causes persistent abnormal foci of alveolar bronchiolization and fibrosis in hamster lung. a.** Experimental layout: 6–8 weeks old hamsters were intranasally inoculated with 10^3 PFU SARS-CoV-2 wild-type strain HK-13 or equal volume of PBS as mock controls. Lung tissues were collected at 120dpi. Dysregulated regeneration in SARS-CoV-2 infected hamster lungs was observed in all hamsters (12/12), and illustrated by H&E-stained sections. Upper image shows lung condensation with blood vessel congestion and multiple abnormal foci, lower image shows abnormal foci of alveolar bronchiolization. **b.** Representative H&E images showing pulmonary consolidation, fibrosis and alveolar bronchiolization in SARS-CoV-2 infected hamster lungs at 120dpi compared to mock control (upper panel). Middle panel: SARS-CoV-2 infected hamsters displayed whole lung condensation and multiple foci from proximal to distal lung regions. Bottom panel: Higher magnification images showing collapsed alveoli, pleurae thickening and alveolar bronchiolization. Black open arrows indicate pleurae thickening. Black triangles indicate alveolar epithelial cell hyperplasia. Scale bar = 500 μm, 200 μm, 100 μm, 50 μm, or 20 μm, respectively.

surrounding bronchioles to distal lung, affecting 4–11.3% of lung area. The cellular morphologies were mainly cuboidal or columnar, consistent with the characteristics of alveolar-bronchiolization (Fig. 1b). However, none of these changes were observed in mock control hamsters, indicating a strong association with previous SARS-CoV-2 infection.

We then investigated the progression process of lung damage caused by SARS-CoV-2 spanning different stages of infection including acute (4, 7dpi), resolving (14dpi) and chronic phase (42, 84 &120dpi). Consistent with our previous findings in acute infection,[22] diffused alveolitis with massive immune cell infiltration at 4dpi, severe alveolar consolidation and hyperplastic regenerative pneumonia at 7dpi were found in SARS-CoV-2 infected hamsters (Fig. 2b & Fig S1). At 14dpi, inflammatory infiltration was largely resolved but still detectable; however, abnormal proliferation foci as ribbons and tubules-like structure started to appear (4/6) (Fig. 2b & Fig S1). At 42dpi, abnormal foci increased in number and size, and were easily observed in peribronchiolar, perivascular regions and distal alveolar area in all the

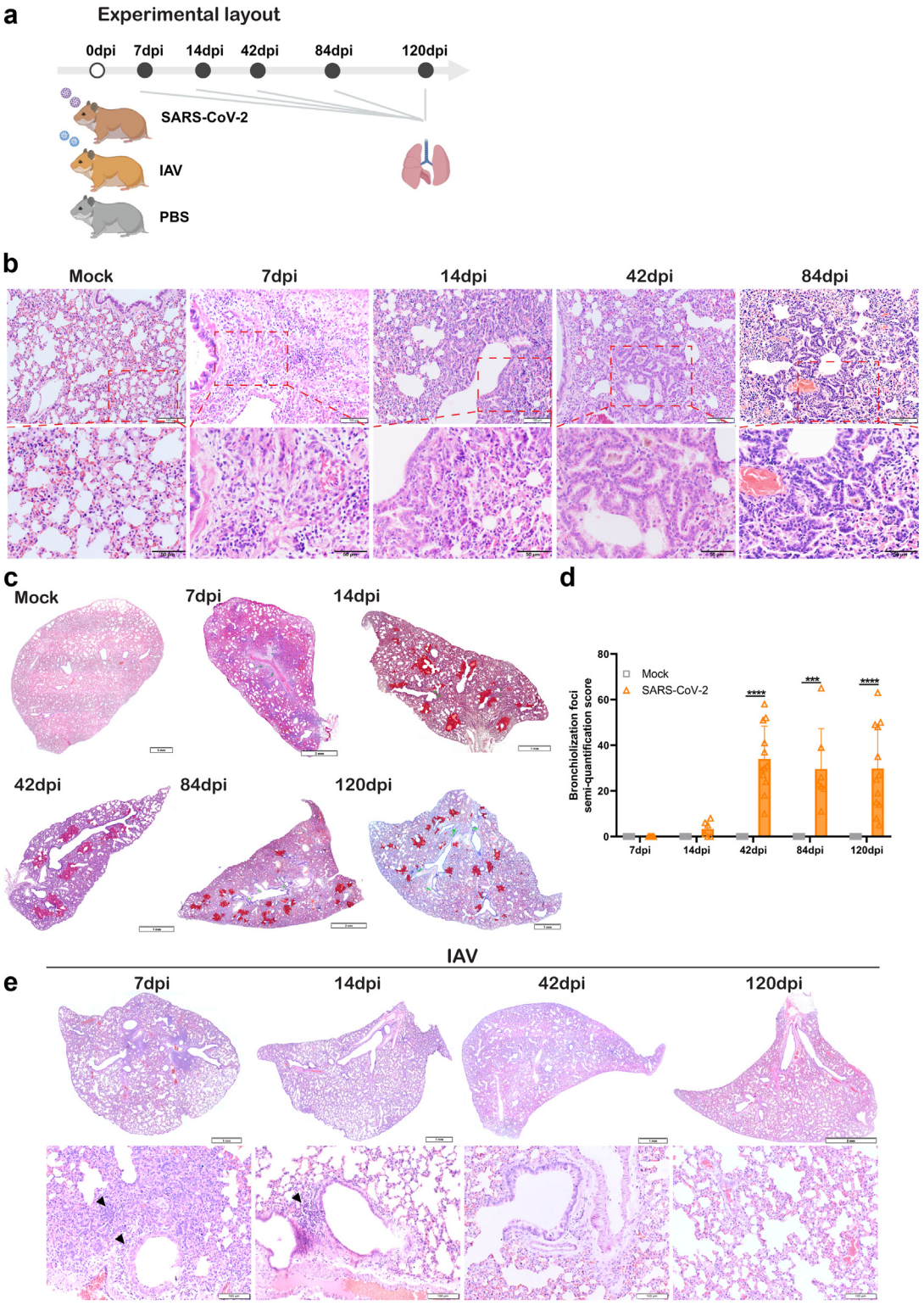

Fig. 2: **Progression dynamic of SARS-CoV-2 infection caused histopathological changes in hamster lung. a.** Experimental layout: 6–8 weeks old hamsters were intranasally inoculated with 10^3 PFU SARS-CoV-2 wild-type strain HK-13, or 10^5 PFU mouse-adapted A (H1N1)pdm09 virus (IAV), or equal volume of PBS as mock controls. Lung tissues were collected at 7, 14, 42, 84 and 120dpi. **b.** Representative H&E images showing

examined lungs (12/12) (Fig. 2b and c). These abnormal foci persisted at 84dpi (7/7) and 120dpi. Semi-quantitative analysis for the number and size of bronchiolization foci yielded a higher score at 42dpi, lower at 120dpi, but had no statistically significant difference (Fig. 2c and d). To be noted, the above-mentioned chronic inflammation and persistent bronchiolization were also observed in the lung after Omicron BA.5 infection 120dpi, though to a less degree comparing with HK-13 virus in terms of affected lung area (Fig. S2a), suggesting that chronic pulmonary damages are not SARS-CoV-2 strain-specific.

To verify whether this chronic lung damage is unique to SARS-CoV-2 infection, hamsters were infected with 10^5 PFU of mouse-adapted A (H1N1) pdm09 (IAV) and lung samples were studied at 7, 14, 42 and 120dpi for comparison with SARS-CoV-2 infection. Consistent with previous findings,[25] at 4dpi (n = 8) and 7dpi (n = 6) H1N1 infected lung showed localized interstitial pneumonia involving every lung lobe examined at various degrees (Fig. 2e), which was generally milder comparing to diffused lung histopathology seen in hamster infected by SARS-CoV-2. H1N1 infection caused inflammation resolved at 14dpi (n = 3) and the lung recovered to normal morphology at 42dpi (n = 5) and 120dpi (n = 5), without bronchiolization foci, which indicates that SARS-CoV-2 causes chronic lung tissue damage but not with influenza virus.

SARS-CoV-2 induced pulmonary fibrosis persisted until 120dpi

Post-COVID pulmonary fibrosis in humans was reported to be the most significant long-term respiratory sequelae.[5] Lung fibrotic changes such as thickened alveolar wall and visceral pleural membrane were observed in SARS-CoV-2 infected hamster lungs at 42 and 120dpi (Fig. 1b). Masson trichrome staining confirmed collagen deposition, prominently in the connective tissue around bronchioles and vessels at 42 and 120dpi (Fig. 3a). Pleural fibrosis was found in 71.4% (5/7) at 42dpi and 42.8% (3/7) at 120dpi. Alveolar septa fibrosis evidenced by increased collagen deposition in Masson trichrome staining were found diffusely distributed in the lung at 42 and 120dpi (7/7, 7/7 respectively). Again, Omicron BA.5 infected hamsters also displayed similar fibrotic changes until 120dpi (Fig. S2b). In IAV infected hamster lungs, collagen deposition was significantly milder compared to SARS-CoV-2 infection, no pleural fibrosis was detected (Fig. 3c). Real-time RT-qPCR assay demonstrated significant upregulation of the genes involving lung tissue fibrosis in SARS-CoV-2 infected lungs (Fig. 3b), including fibroblast growth factor (FGF)1, FGF2 and FGF7. Transforming growth factor-β (TGF-β)1, a well-known major profibrogenic cytokine,[36] had a 10-fold increase after SARS-CoV-2 infection compared to IAV at 42dpi. Imbalanced expression of Matrix metalloproteinases (MMPs) and their specific tissue inhibitors of metalloproteinase (TIMPs) is closely involved in pulmonary fibrosis and fibrolysis.[37] In line with this, at 42dpi, MMP2 and MMP9 mRNA level didn't increase much while TIMP1 and TIMP2 were highly upregulated in SARS-CoV-2 infection than in IAV infection (Fig. 3b). At 120dpi, both MMPs and TIMPs were elevated in SARS-CoV-2 infected lungs, whereas only slight upregulation of TIMP2 and TIMP3 were observed at 120dpi of IAV infection.

In line with above histological changes and RT-qPCR results, bulk RNAseq profiles of hamster lungs at 42dpi after SARS-CoV-2 or IAV infection further revealed significant upregulation of genes related to epithelial cell proliferation, fibroblast growth factor signaling and TGFβ signaling pathways in SARS-CoV-2 infected lungs (Fig. 3d). In addition, genes related to canonical WNT signaling were also upregulated (Fig. 3e). These suggest that some molecular pathways involving tissue regeneration, remodeling and fibrosis process are all highly activated at chronic stage in SARS-CoV-2 infected lungs.

Residual SARS-CoV-2 virus persisted in hamster lungs accompanied with chronic inflammatory responses

Consistent with previous reports,[22,38] highly increased expression of IL6, TNFα, IFNγ, CXCL10 and CCL3 mRNA were detected in the lung tissue at 7dpi after SARS-CoV-2 infection. Unexpectedly, these inflammatory cytokine/chemokines displayed a prolonged upregulation at 42dpi, only decreased but remained higher than mock at 84dpi (Fig. 4a). Notably, chronic inflammatory cytokine IL33 and IL13 were significantly upregulated at 42dpi or 120dpi (Fig. 4b). Fibrinogenβ had about 20-fold increase at 120dpi compared to mock control group. On the contrary, IAV-infected hamsters showed elevated IFNγ, TNFα, CXCL10 and CCL3 mRNA levels at 7dpi and gradually decreased to normal level at 42dpi. These findings indicate that sustained

the prominent histological changes of SARS-CoV-2 infected hamster lungs at 7, 14, 42, 84dpi, and mock control lungs. **c.** Representative full scan H&E image of SARS-CoV-2 infected hamster lung lobe at 7, 14, 42, 84, 120dpi, and mock control. Red highlighted region indicate bronchiolization foci, which were observed in all the hamsters examined from 42dpi onward: 42dpi (12/12), 84dpi (7/7) and 120dpi (12/12). The green highlighted region indicate infiltration. **d.** Semi-quantification score of bronchiolization foci. n = 5 for mock control, 6 for 14dpi, 7 for 84dpi, 12 for 42&120dpi. **e.** Representative H&E images of IAV infected hamster lungs at 7, 14, 42 and 120dpi. Triangles indicate cell infiltration. Scale bar = 2 mm, 1 mm, 100 μm, or 50 μm, respectively. Data represented mean ± SD. ***p < 0.001, ****p < 0.0001 by Two-way ANOVA with Tukey's multiple comparisons test (d).

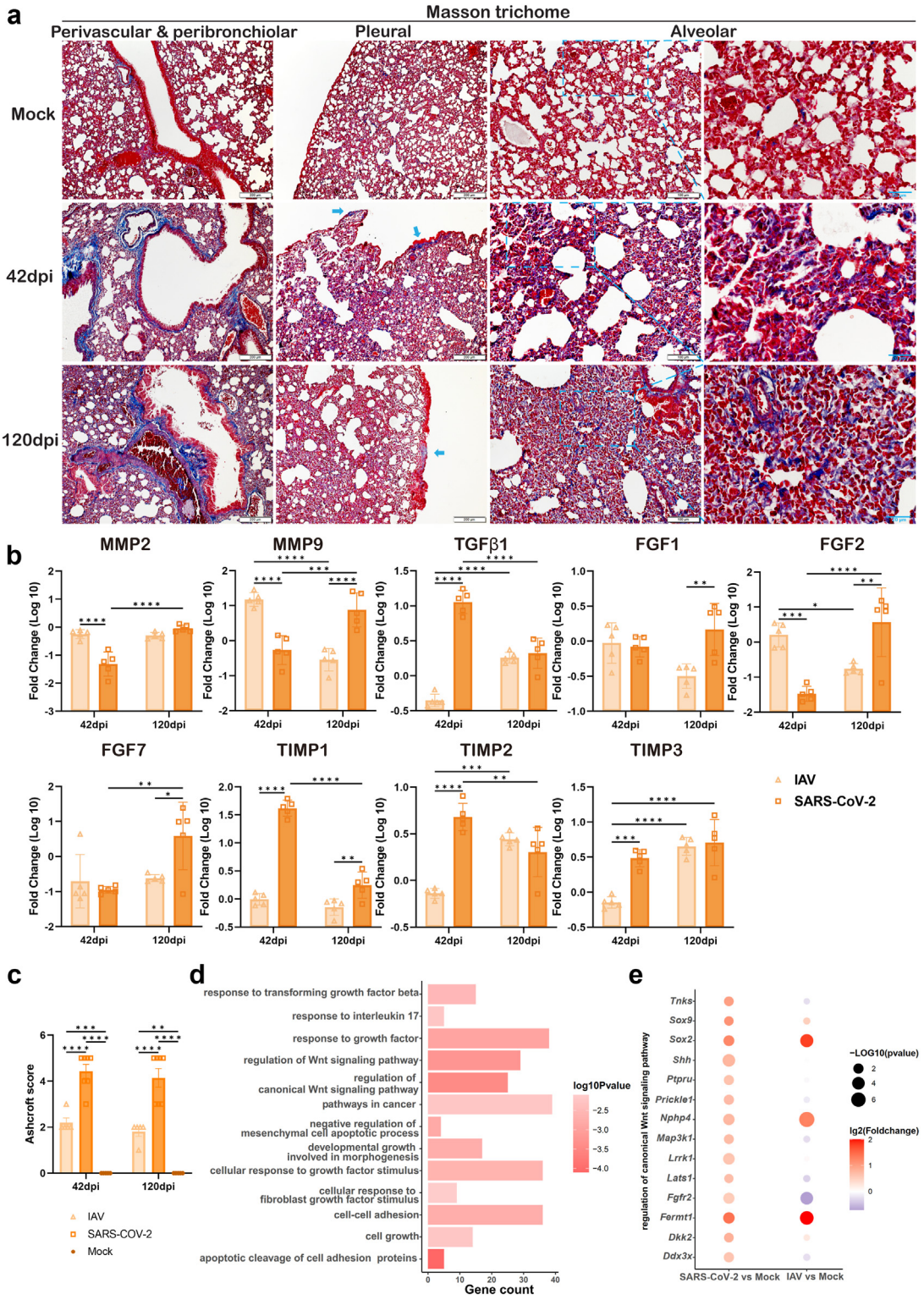

***Fig. 3:* SARS-CoV-2 infection causes persistent fibrosis in hamster lung. a.** Representative images of Masson trichrome stained lung of mock or SARS-CoV-2 infected hamsters at 42 and 120dpi. Left panel: Representative images showing dramatically increased collagen deposition in perivascular and peribronchiolar tissue in SARS-CoV-2 infected hamsters (blue color). Second left panel: Representative images showing pleural fibrosis in SARS-CoV-2 infected hamsters. Blue arrows indicate thickened visceral pleural membrane. Right two panels: Representative images

inflammatory responses persisted long after acute phase of SARS-CoV-2 infection.

Now the obvious question is whether the observed lung chronic inflammation is associated with presence of virus residue in the lung. To this end, we detected SARS-CoV-2 virus with multiple methods. RT-qPCR detection RdRp gene showed that viral load peaked at 4dpi, then declined at 7dpi, remained detectable in 8/12 (66.7%) of the hamster lungs at 42dpi, 6/7 (85.7%) at 84dpi and 8/12 (66.7%) at 120dpi, respectively. As for IAV infected hamster lungs, the results from M gene RT-qPCR showed complete clearance of virus at 14dpi (Fig. 4c).

To detect viral antigen, we performed immunohistochemistry (IHC) and immunofluorescence (IF) staining for SARS-CoV-2 N antigen and IAV N antigen in lung sections, respectively. As expected, SARS-CoV-2 and IAV infected lungs both displayed extensive expression of viral antigen at 4dpi, respectively. Both IHC and IF staining showed scattered SARS-CoV-2 N positive cells in all the lungs samples at 42, 84 and 120dpi. Furthermore, double IF staining for macrophage marker Ionized calcium binding adapter molecule 1(Iba1) and SARS-CoV-2 N antigen showed double positive cells around terminal bronchiole at 42, 84 and 120dpi, while no IAV N antigen was detectable at 14, 42 and 120dpi (Fig. 4d and e). Semi-quantitation indicated that more than 85% of SARS-CoV-2 N+ cells were Iba1 positive, suggesting lung macrophages are still harboring SARS-CoV-2 long after recovery from acute infection. SARS-CoV-2 N+ cells in or around bronchiolization foci were also detected, which may suggest a possible association of virus residue to bronchiolization (Fig. S3), which needs further study. Taken together, we prove that unlike influenza infection, acute SARS-CoV-2 infection could leave behind viruses or viral components in hamster lungs for prolonged period of time.

Alveolar AT2 cell replenishment in lung regeneration after SARS-CoV-2 infection

AT1 and AT2 cells are both the primary targets of SARS-CoV-2 virus, while only AT2 cells are considered as progenitors to replenish the damaged alveolar epithelium after injury.[10] To understand the process of lung tissue regeneration, we first evaluated the dynamic changes of AT2 cells upon SARS-CoV-2 infection. Dual IF staining of AT2 cells with SPC and Ki67 at different time points showed AT2 cell number and percentage decreased significantly at 4dpi due to virus caused cell death and massive influx of immune cells to the lung, the AT2 cells rapidly increased at 7dpi and resumed to the level as of mock control at 14dpi (Fig. 5a and b). The percentage of Ki67+ proliferative AT2 cell increased significantly at 4dpi, peaked at 7dpi, remained high at 14dpi (Fig. 5a and c), which indicated that lung infection activated the proliferation of undamaged AT2 cells. AT2 proliferation rate (Ki67 positivity) returned to base-line level from 42dpi to 120dpi (Fig. 5c), indicating no persistent activation of AT2 cells. Notably, AT2 cells were rarely detected in bronchiolization foci from 14 to 120dpi, suggesting that activated AT2 cells are not the origin of the alveolar-bronchiolization.

CK14+ basal cells participated airway regeneration and alveolar-bronchiolization after SARS-CoV-2 infection

Next, we systematically investigated the role of CK14+ basal cell in SARS-CoV-2 infected lung regeneration. In mock control hamster, only a few CK14+ basal cells could be seen in the airway, but none in alveoli. At 4 and 7dpi after SARS-CoV-2 infection, the number of CK14+ basal cells increased remarkably in both bronchioles and alveoli with most CK14+ cells double expressing Ki67+CK14+ (Fig. 6a and e). A few of CK14+SPC+ cells were detected at 7dpi suggested CK14+ basal cells may contribute to AT2 cells repair to some extent (Fig. 6b). At 14 dpi, CK14+ basal cells were only detected in bronchioles in IAV infected hamster lung (Fig. S4). On the contrary, in SARS-CoV-2 infected lung, the number of CK14+ basal cells decreased in bronchiole accompanied with histological morphology showing repaired airway epithelium, while they remained as clusters in alveoli surrounding bronchioles (Fig. 6a). Some of them were co-expressing Ki67 until 42dpi, indicating persistent activation of CK14+ basal cells. Within these cell clusters, CK14+SCGB1A1+ or CK14+Tubulin+ cells were frequently observed at 14dpi (Fig. 6c and d), suggesting these CK14+ basal cells differentiated into club cells or ciliated cells in alveoli.

To further characterize the cell types in the bronchiolization foci, IF staining was performed for club cells with SCGB1A1 and ciliated cells with Tubulin. SCGB1A1+ club cells and Tubulin+ ciliated cells were only found in the airway epithelium of mock control. In acute SARS-CoV-2 infected lungs, the airway luminal sloughed epithelial cells expressing SCGB1A1 and Tubulin at 4dpi, indicating infection caused death of club and ciliated cells (Fig. 7a). Only from 14dpi onward, increased number of SCGB1A1+ cells and Tubulin+ cells were easily observed, forming gradually

and magnified images showing increased collagen deposition in alveolar wall in SARS-CoV-2 infected hamsters. Scale bar = 200 μm, 100 μm, or 20 μm, respectively. **b.** Relative mRNA expression levels of genes, MMPs, TIMPs, FGFs and TGF in the lung tissues of SARS-CoV-2 or IAV infected hamsters. n = 5. **c.** Semi-quantification of collagen deposition degree using Ashcroft score. n = 5 for IAV groups and 7 for other groups. **d.** Upregulated pathways in SARS-CoV-2 infected hamster lungs at 42dpi by RNAseq analysis. **e.** Differential expression of genes in regulation of canonical WNT signaling pathway in SARS-CoV-2 infected hamster lungs at 42dpi by RNAseq analysis. Data represents mean ± SD. *p < 0.05, **p < 0.01, ***p < 0.001, ****p < 0.0001 by Two-way ANOVA with Tukey's multiple comparisons test (b and c).

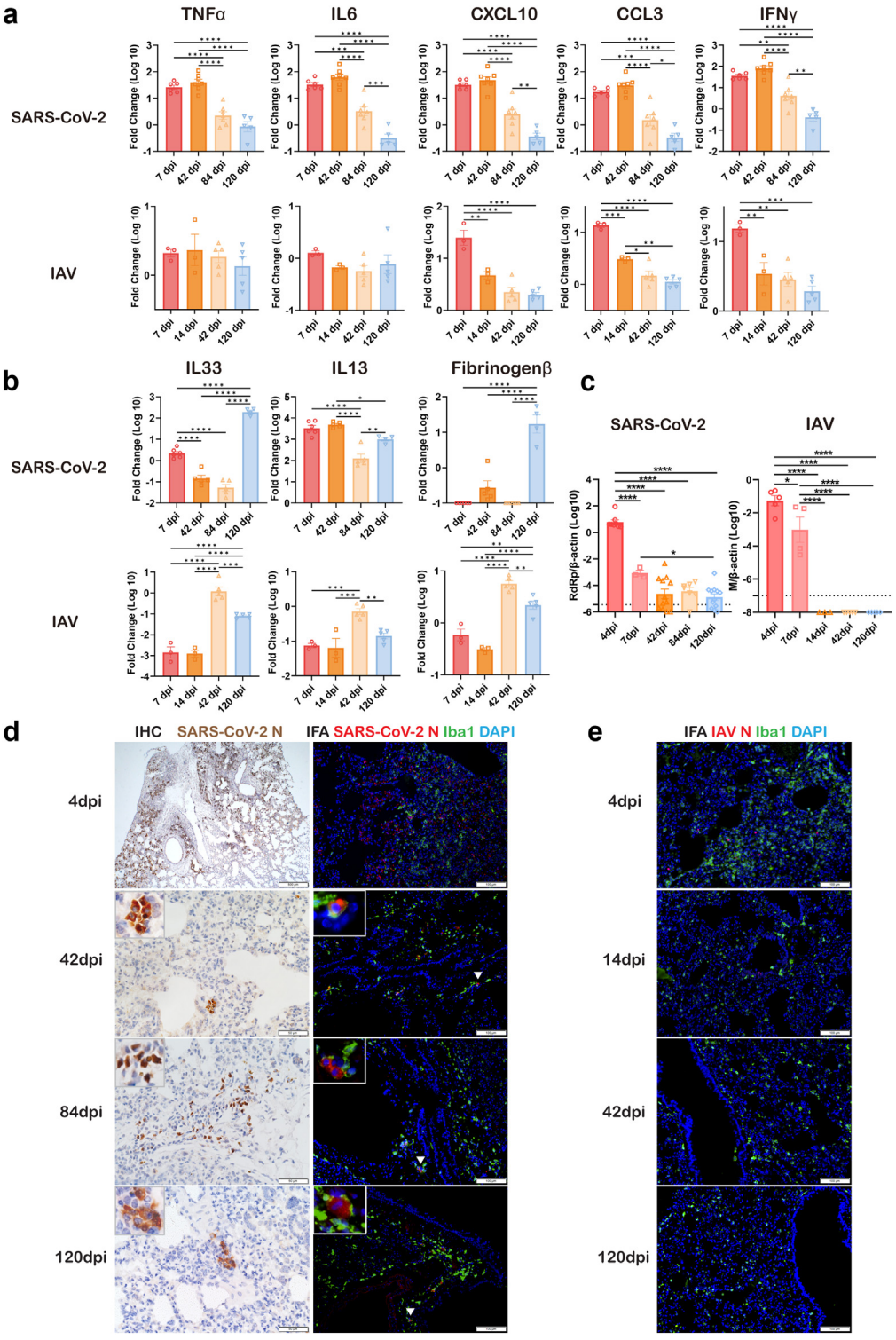

Fig. 4: **Sustained inflammatory responses and virus persistence in hamster lung after SARS-CoV-2 infection. a.** Relative mRNA expression levels of proinflammatory cytokines/chemokines in the lung tissues of SARS-CoV-2 and IAV infected hamsters from 7dpi to 120dpi. n = 3 for IAV 7&14dpi, 5 for IAV 42&120dpi and SARS2 120dpi, 6 for SARS2 7dpi, 7 for SARS2 42&84dpi. **b.** Relative mRNA expression levels of chronic inflammatory mediators in the lung tissues of SARS-CoV-2 and IAV infected hamsters. n = 3 for IAV 7&14dpi, 5 for IAV 42&120dpi and SARS2 42&84dpi, 6 for SARS2 7dpi, 4 for SARS2 120dpi. **c.** Viral load of SARS-CoV-2 RdRp (left) and influenza M (right) in the lung tissues at different

enlarged foci with ribbon-like or honeycomb-like structures in alveoli (Fig. 7b). Together with the features shown in H&E-stained lung sections, we confirmed that SCGB1A1+ club cells and Tubulin+ ciliated cells are the major cellular components of bronchiolization foci in SARS-CoV-2 infected hamster lung. Collectively, these temporal cell type identifications demonstrated that CK14+ basal cells served as major progenitors in the repair of bronchiolar epithelium damaged by SARS-CoV-2 infection, meanwhile they migrated to alveoli, differentiated and formed bronchiolization foci.

Notch pathway highly activated in chronic phase of SARS-CoV-2 infection

First, by RT-qPCR assay, we determined the mRNA levels of Notch and some Notch pathway related genes in the lung tissues at 42dpi and 120pdi after SARS-CoV-2 infection. Notch1 and Notch3 were found significantly elevated 30-40-fold and 80-fold at 42dpi and 120dpi, respectively, when compared to mock controls (Fig. 8a). A significant increase of Notch2 was only detected at 42dpi. Strikingly, Jagged Canonical Notch Ligand (Jag)1 showed a 150–250-fold increase. Hey1 (Hairy/Enhancer of Split related to YRPW motif 1) also highly elevated, while Hes 1(Hairy/Enhancer of Split1) decreased. Notch pathway regulatory gene Sox2 (SRY-related HMG-box 2) increased at 120dpi. On the contrary, IAV infected hamsters only showed less than two-fold increase of Jag1, no other detectable changes in lung at 42 or 120dpi.

To detect Notch3 protein, IF staining showed sporadic Notch3 positive cells appeared in alveoli of SARS-CoV-2 infected lung at 14dpi. However, intensively stained Notch3 positive cells were shown in the lung sections of 42, 84 and 120dpi, which are located in the bronchiolization foci (Fig. 8b). Closer examination identified nuclear localization of Notch3 protein in some of the cells (Fig. 8c), which further indicates activation of Notch3. Moreover, Hes1 protein was also highly expressed in bronchiolization foci at 42 and 120dpi (Fig. 8d). Collectively, our data indicate continuous and persistent activation of Notch pathways in the lung during the chronic phase of SARS-CoV-2 infection.

Transcriptional changes overlapping alveolar-bronchiolization region in the lung

To better understand the gene transcriptional changes in relation to alveolar-bronchiolization, we conducted spatial transcriptomic analysis for hamster lung samples collected at 120dpi. Six tissue regions were identified and selected to represent abnormal (bronchiolization region in red circles), or normal (non-bronchiolization region in black circles) alveolar structure based on histological features observed in the H&E section (Fig. 9a). The transcriptomic profiles were compared between the abnormal and the normal tissue regions. Firstly, cell type signature genes for lung epithelial cells,[8] including AT1, AT2, ciliated cells and club cells were applied for spatial mapping. For instance, *Ccdc39*, which is highly expressed in ciliated cells,[39] was abundantly detected in abnormal regions (Fig. 9b). *Foxj1*, which induces basal cells differentiation to ciliated cells, was detected only in abnormal regions (Fig. 9b & Fig. S5). Higher expression of ciliated cell and club cell marker genes, together with lower expression of AT1 and AT2 cell marker genes were observed in abnormal regions than in normal regions (Fig. 9c). This data from transcriptional level proved the aberrant cellular composition in the abnormal alveolar regions. Secondly, pathway enrichment analysis of the DEGs between the normal and abnormal regions revealed the upregulation of genes associated with positive-regulation of cell growth, position-regulation of GTPase activity, Wnt signaling pathway, NF-kappaB and ERBB signaling pathways in the abnormal regions (Fig. 9d). Moreover, genes associated with positive regulation of Notch signaling pathway (GO: 0045747) were also upregulated in the abnormal regions (Fig. 9e). Taken together, spatial-specific transcriptomic data provide further evidence supporting dysregulated lung regeneration after SARS-CoV-2 infection.

Interestingly, we also identified significant upregulation of several pro-tumor genes or genes positively regulating cell cycles, including tubulin beta 4B class IVB (*Tubb4b*), syntaxin binding protein 4 (*Stxbp4*), growth factor receptor bound protein 14 (*Grb14*), Myeloid leukemia factor 1 (*Mlf1*), Mucin 1 (*Muc1*) and P53 Apoptosis Effector Related to PMP22 (*Perp*) were detected in abnormal regions (Fig. 9f). Moreover, extensive signals of Mlf1 and Sox2 were observed in the cells of bronchiolization foci (Fig. 10).

Discussion

A substantial proportion of COVID-19 patients developed physical and/or mental conditions long after recovering from SARS-CoV-2 acute infection, some of them manifested as respiratory symptoms which may or may not accompany with radiologically detectable lung abnormalities including inflammation, ground-glass opacities or fibrotic changes.[4,5] To investigate the

time points after infection. n = 3 for SARS2 7dpi and IAV 14dpi; 4 for IAV 7dpi; 5 for IAV 4, 42&120dpi; 7 for SARS2 84dpi; 8 for SARS2 4dpi; 12 for SARS2 42&120dpi. Dashed lines indicate as cut-off line determined by mock controls. **d.** Representative immunohistochemistry stained SARS2-CoV-2 N protein (left panel) and double immunofluorescence-stained N protein (red) and macrophage marker Iba1 (green) (right panel) in SARS-CoV-2 infected hamster lung. Triangles indicate positive cells which were magnified in each insert. **e.** Double immunofluorescence stained IAV N protein (red) and macrophage marker Iba1 (green) in IAV infected hamster lung. Scale bar = 100 μm. Data represents mean ± SD. *p < 0.05, **p < 0.01, ***p < 0.001, ****p < 0.0001 by One-way ANOVA with Tukey's multiple comparisons test (a–c).

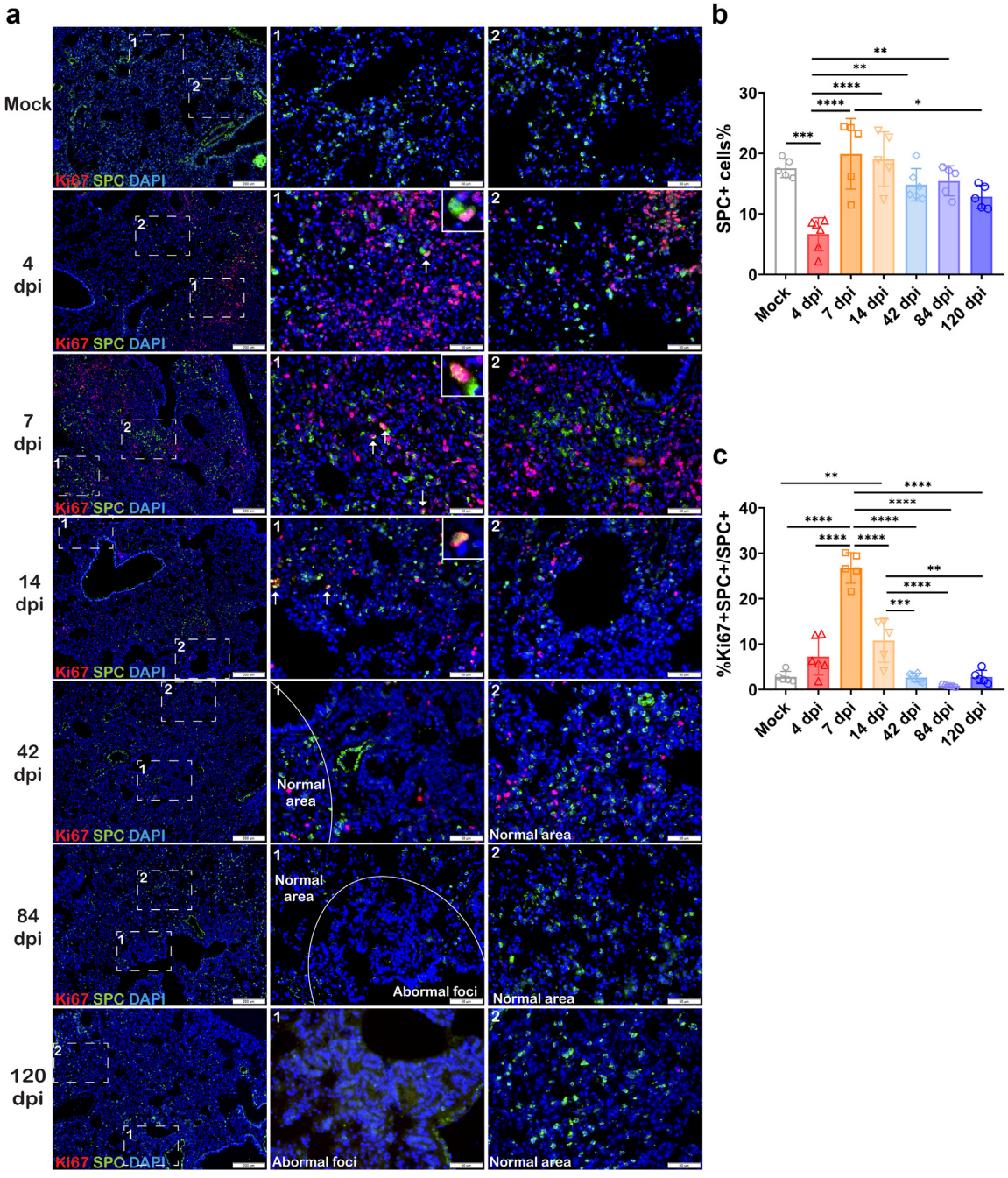

Fig. 5: **Alveolar AT2 cell regeneration in SARS-CoV-2 infected hamsters**. **a.** Representative images of immunofluorescence stained Ki67 (red) and SPC (green) in SARS-CoV-2 infected hamster lungs. Numbered squares were magnified on the right-side. White arrows indicate Ki67 and SPC double positive cells illustrated in the inserts. Scale bar = 200 μm or 50 μm. **b.** Percentage of SPC+ AT2 cells in total cells of mock and SARS-CoV-2 infected hamster lung. n = 6 for 4&42dpi, 5 for other groups. **c.** Percentage of proliferative AT2 cells (Ki67+ SPC+/SPC+) in mock or SARS-CoV-2 infected hamster lungs. n = 6 for 4&42dpi, 5 for other groups. Data represents mean ± SD. *p < 0.05, **p < 0.01, ***p < 0.001, ****p < 0.0001 by One-way ANOVA with Tukey's multiple comparisons test (b and c).

histopathological changes underlying the chronic lung diseases, we utilize a well-established hamster model and demonstrate SARS-CoV-2 infection led to chronic lung tissue inflammation and fibrosis with residual virus residing in lung macrophages beyond 120dpi. Excessive proinflammatory cytokines responses caused

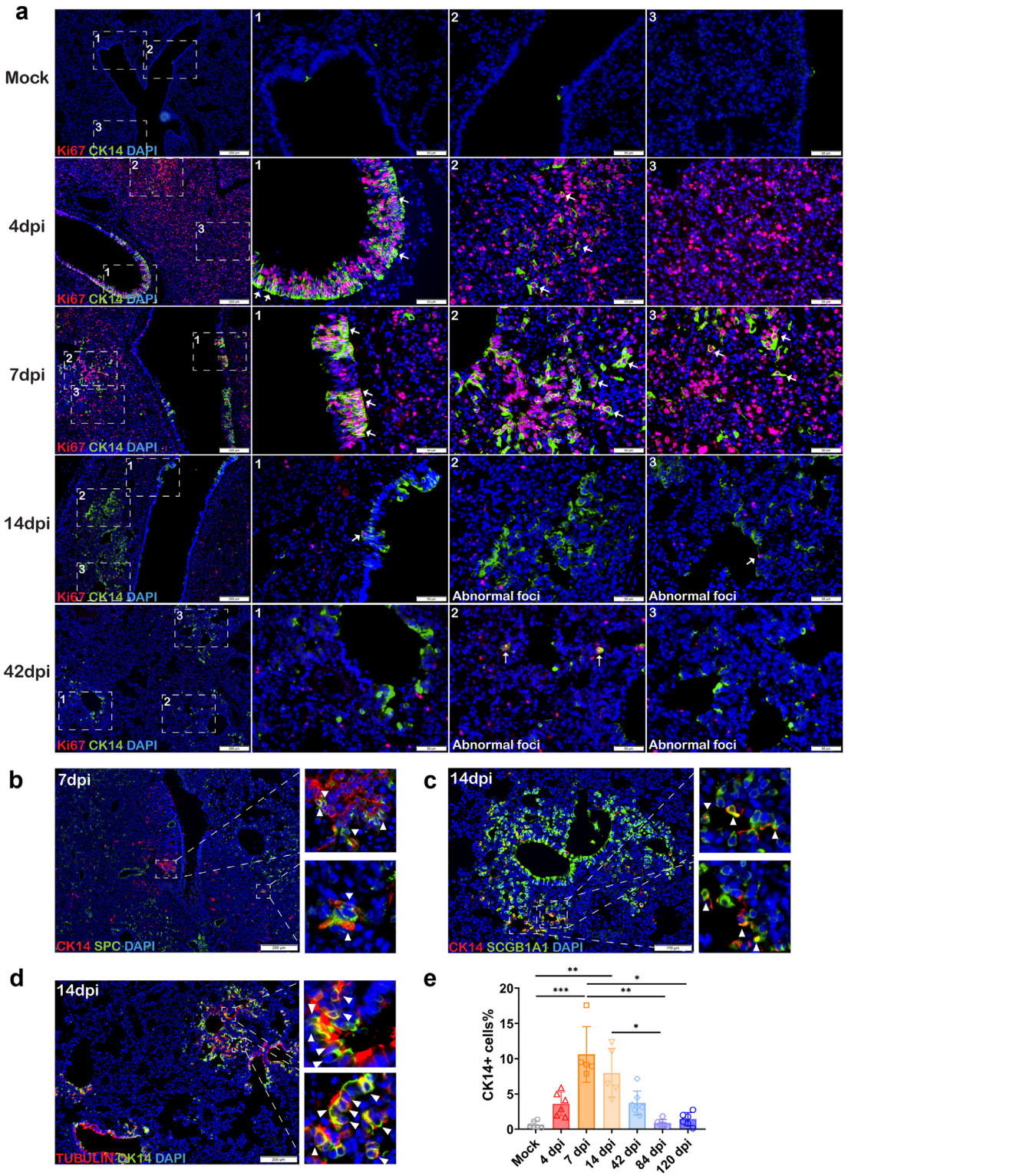

***Fig. 6:* CK14+ basal cells actively proliferated, differentiated in lung regeneration and bronchiolization in SARS-CoV-2 infected hamsters.** **a.** Representative images of immunofluorescence stained Ki67 (red) and CK14 (green) in SARS-CoV-2 infected hamster lungs from 7dpi to 42dpi. Scale bar = 200 μm or 50 μm. Squared area 1 indicates bronchioles, area 2 and 3 indicate alveoli. White arrows indicate Ki67 and CK14 double positive cells. **b.** Representative image of immunofluorescence stained CK14 (red) and SPC (green) in SARS-CoV-2 infected hamster lung

by SARS-CoV-2 infection sustained up to 42 days followed with increased expression of chronic inflammatory mediators. Alveoli regeneration process following SARS-CoV-2 infection was disrupted by dysregulated CK14+ basal cells activation, migration and differentiation into SCGB1A1+ club cells and Tubulin+ ciliated cells, forming alveolar-bronchiolization that persisted until 120dpi. However none of these chronic changes were observed in the A (H1N1)pdm09 infection. This study shed lights for understanding lung long-COVID symptoms in humans. Furthermore, our investigation indicated the involvement of continuous upregulation of Notch pathway and related genes in maintaining the alveolar-bronchiolization.

The Syrian hamster SARS-CoV-2 model simulated the lung pathology very well in human COVID-19, inflammatory tissue damages peak at 4dpi and start to resolve at 7dpi and recovered at 14dpi.[22,24] We found that after acute infection resolved at 42dpi, the proinflammatory cytokines/chemokines (IL6, TNFα, CXCL10 and CCL3) remained as high as 7dpi, then gradually reduced but not diminished, remained above baseline level until 120dpi when IL33, IL13 and Fibrinogenβ were highly upregulated in the lung. This indicated the acute inflammation was not resolved completely while developing into a state of chronic inflammation. As in COVID-19 patients, our previous short-term animal study and many others showed that SARS-CoV-2 virus shedding from oral or fecal route when the host mounted effective adaptive immunity.[24,40] However, we detected SARS-CoV-2 RNA and proteins in hamster lungs sampled at 42, 84 and 120dpi though with low copies of RNA and scattered antigenexpressing cells, this proves SARS-COV-2 lingered in the lung long after the host recovered from acute infection. Human clinical reports also indicated SARS-CoV-2 virus residues in various human organs long after acute disease.[41] Furthermore, we proved that the virus mainly resides in lung macrophages as 85% of the viral N protein expressing cells are macrophage. In human autopsy, SARS-CoV-2 N protein was detected in macrophages in secondary lymphoid tissue and SARS-CoV-2 RNA was found in CD68+ macrophages in lung tissues.[42,43] Another longitudinal study in cynomolgus macaques showed that replication-competent virus in bronchoalveolar lavage fluid macrophages 6 months post SARS-CoV-2 infection without evidence of infectious virus produced.[44] We currently do not have evidence regarding whether the virus is capable of replication in hamster macrophages either. Or, whether the virus replication was merely suppressed by host adaptive antiviral immunity? Whether it will "rebound" when the immune response wanes down or in other circumstances of impairment of host immune function? Further investigations are warranted. Nevertheless, virus persistence in macrophages is unarguably an inflammation inducer that contributes to sustained inflammation in the lung, at least in part. On the other hand, persistent viral components in macrophages could engage with pattern-recognition receptors and induce cytokine responses. Repeated stimulation of pattern-recognition receptors might lead to effector activity, exhaustion of virus-specific T cells and B cells, which will further result in tissue damage or cytopathology.[41] SARS-CoV-2 proteins are documented to dysregulate host signaling pathways through disrupting host metabolic, genetic and epigenetic regulations,[45] which may also contribute to chronic inflammation.

Prolonged inflammation and presence of viral components in the lung will undoubtedly affect the process of lung tissue regeneration. Our transcriptomics analysis indicated significant upregulation of fibroblast growth factor and TGFβ signaling pathway related genes in SARS-CoV-2 infected lungs at 42dpi. At this time point, significant upregulation of TGF-β1, TIMP1 and TIMP2 was also detected by RT-qPCR. When disease progressed to 120dpi, there were high level expressions of FGF1, FGF2 and FGF7 in the lungs. These transcriptional changes indicate the prolonged and imbalanced activation of pulmonary tissue repair and fibrotic pathways. In keeping with this, widespread collagen deposition in the visceral pleural membrane, lung interstitial connective tissue and alveolar septa were observed microscopically. These findings in hamsters provide histological support for clinical manifestations in human.[5,6] Lung tissue fibrosis was observed in COVID-19 patients as early as 3 weeks after the onset of symptoms. It is reported that 38% of COVID-19 patients displayed lung fibrosis features from CT scan at a median of 54 days after disease onset, and 9% of them deteriorated up to 8 months discharged from hospital.[4,46] Currently, information in humans for long periods of time is still accumulating. However, 15 years' observational data on SARS patients showed that the residual lung abnormalities including fibrotic changes reduced within the first 1 year after recovery but remained in the following 14 years.[47] It is likely that progression of post-COVID lung fibrosis is similar with SARS, which may last for a long time. Our observation in hamster lung supports this notion.

at 7dpi. White triangles indicated CK14 and SPC double positive cells. Scale bar = 200 μm. **c and d**. Representative image of immunofluorescence stained CK14 (red) and SCGB1A1 (green) (c) or CK14 (red) and Tubulin (green) (d) in SARS-CoV-2 infected hamster lung at 14dpi. White triangles indicate double positive cells. Scale bar = 200 μm or 100 μm. **e.** CK14+ basal cells percentage in total cells of mock or SARS-CoV-2 infected hamster lung. n = 6 for mock, 4dpi, 84&120dpi; 5 for 7&14dpi; 7 for 42dpi. Data represents mean ± SD. *p < 0.05, **p < 0.01, ***p < 0.001, by Kruskal–Wallis test with Dunn's multiple comparisons test.

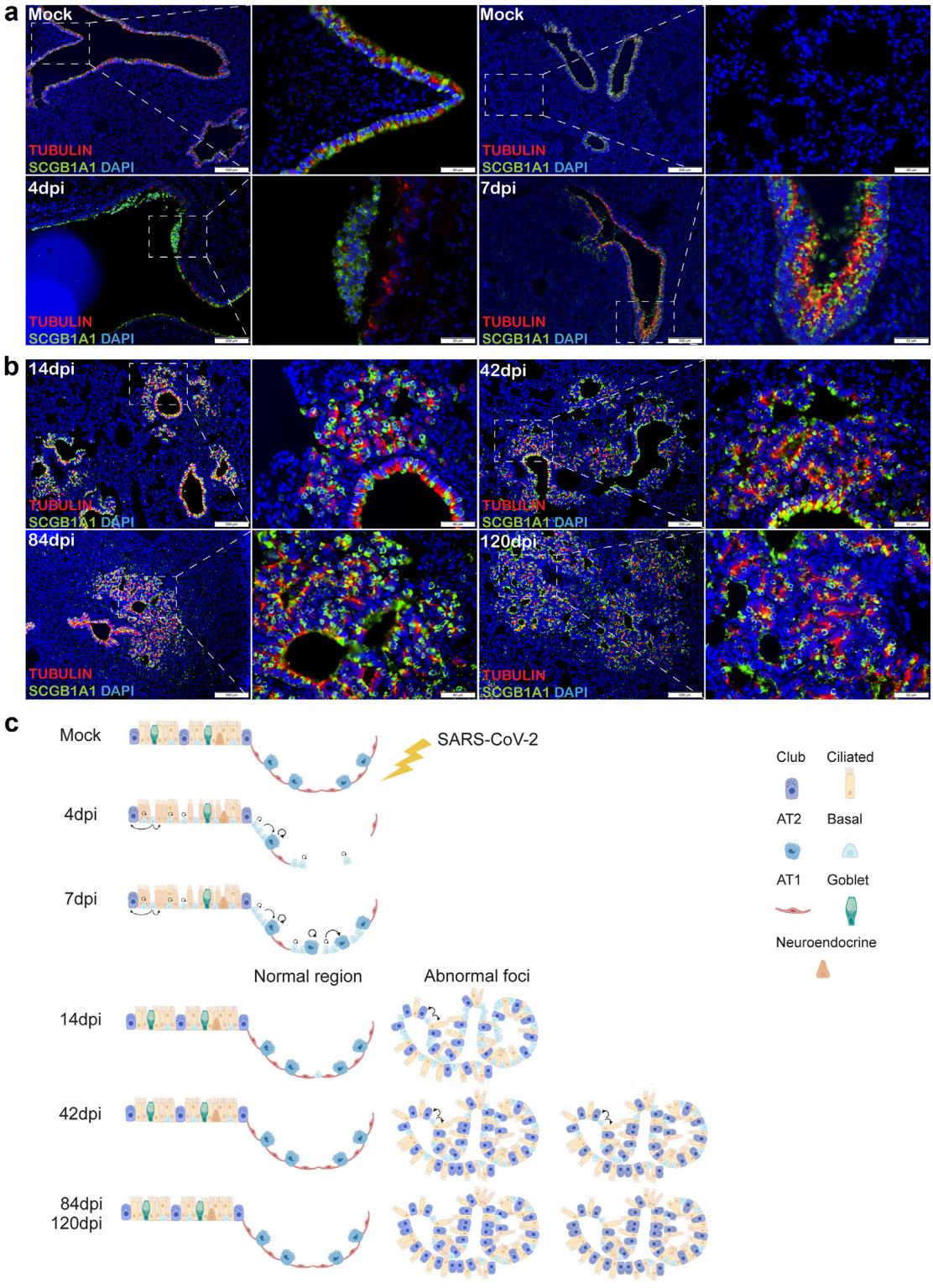

***Fig. 7*: Bronchiolization foci is mainly composed of ciliated and club cells in SARS-CoV-2 infected hamster lung. a.** Representative images of double immunofluorescence-stained Tubulin (red) and SCGB1A1 (green) in airway epithelium of mock or SARS-CoV-2 infected hamster lungs at 4 and 7dpi. Scale bar = 200 μm or 50 μm. **b.** Representative image of double immunofluorescence-stained Tubulin (red) and SCGB1A1 (green) in the airway and alveolar-bronchiolization foci in SARS-CoV-2 infected hamster lungs at 14, 42, 84 and 120dpi. Scale bar = 200 μm or

The most remarkable chronic histological abnormality we found in the lung of SARS-CoV-2 infected hamster was the multifocal ribbon-like or honeycomb-like epithelial structures. This bronchiolar epithelium–like structure was characterized as alveolar-bronchiolization, which has also been reported by others shortly after the hamsters recovered from SARS-CoV-2 infection.[8,48,49] Our hypothesis is that severely destructed multiple types of lung cells, from airway to alveoli, in SARS-CoV-2 acute infection activate distal airway progenitor cells. The molecular niche created by persistent inflammation dysregulates the proliferation and differentiation of these progenitor cells and alters the process of tissue regeneration. To prove this, through analysis of serial lung samples, we found that AT2 cells were rapidly activated and proliferated upon the severe loss of viral infected cells to replenish the damage alveoli. This is in agreement with the role of AT2 cells' self-renewal in alveoli regeneration and tissue homeostasis.[11] From 7dpi onward, AT2 cell number returned to baseline, suggesting AT2 cells regeneration remained relatively intact. Here we did not evaluate whether AT2 cells function as a progenitor to replenish the lost AT1 cells. But Heydemann and colleagues[8] reported that in SARS-CoV-2 infected hamster lung, this process was impaired with a prolonged state of alveolar differentiation intermediate (ADI) cells expressing CK8+. They further suggested that multipotent CK14+ basal facilitate alveolar regeneration upon SARS-CoV-2 infection, however, the longest observation time in their study was 14dpi. Our longitudinal data indicate that CK14+ cells played limited roles in AT2 cell replenishment when they migrated into alveoli, though we also observed a few CK14+ basal cells co-expressing SPC at the early time of tissue repair.

Studies in human and mice showed CK5+ basal cells participate in alveoli regeneration.[12,19,50] To this end, proliferated CK5+ basal cells formed cell clusters termed "keratin 5 pods", a common feature of epithelial remodeling process after alveoli damage.[12,19,50] However, consistent with a previous report on hamster model,[8] we were unable to detect many CK5+ cells in mock or infected hamster lungs. We assumed that CK14+ basal cells in hamster lungs should be functionally equivalent to CK5+ basal cells in human and mice. Increased number of CK14+ basal cells were detected as early as 4dpi in bronchiolar epithelium. At 14dpi, CK14+ basal cells decreased sharply in bronchiolar epithelium, where was restored completely, while the CK14+ basal cells present in alveoli continued to proliferate and differentiate to become club cells and ciliated cells instead of differentiating into AT2 or AT1 cells. This implies the microenvironment of lung altered CK14+ basal cells differentiation.

Complex molecular pathways have tight regulation on the self-renewal and differentiation of progenitor cells.[14] Notch signaling pathways play important roles in regulating lung basal cell differentiation and lung regeneration.[14,51,52] Notch3 activation primes basal cells to suprabasal cells,[52] which subsequently differentiate to club cells or goblet cells through Notch1/2 and Hey signaling activation.[52] It has been previously shown that basal cells can directly differentiate to ciliated cells during lung repair through Notch2 activation and Sox2 upregulation.[53] Sustained Notch activation promotes basal cells differentiation toward club cell lineage and inhibits basal cell trans-differentiation to alveolar epithelia cells.[12,14] In SARS-CoV-2 infected hamster lungs, elevated expression of Notch1, Notch3, Hey1, Jag1 and Sox2 at 120dpi is in line with these previous reports. Furthermore, spatial transcriptomic data showed that genes associated with positive regulation of Notch signaling pathways were upregulated in the abnormal foci. Consistent with our findings, Notch signaling was upregulated at transcriptional level in SARS-CoV-2 infected juvenile macaque lungs at 14dpi, no lung pathological was described,[54] which may be due to the short observation period. Notch activation was also observed in influenza virus infection in mice.[12] We believe in SARS-CoV-2 infection, in addition to the microenvironment that may affect CK14+ basal cell activities, dysregulation of Notch and Wnt signaling, TGF-β signaling and sustained cytokine/chemokine expression would lead to aberrant differentiation of CK14+ basal cells, resulting in persistent alveolar bronchiolization.

Different from SARS-CoV-2 infection, alveolar-bronchiolization was not observed in the hamster infected with A (H1N1)pdm09 influenza virus infection. Syrian hamster is also susceptible to this mouse adapted A (H1N1)pdm09 strain, which induced interstitial pneumonia after intranasal inoculation.[25] Even with 10^5 PFU dose (100-times more than SARS-CoV-2), the tissue damage is milder compared with SARS-CoV-2 infection, alveolar damage is less diffuse with less fluid leakage in the alveolar sac. A (H1N1)pdm09 caused lung inflammation resolved completely at 14dpi with no evidence of uncleared virus, nor chronic inflammatory lesion during our longitudinal study until 120dpi. Previously, Vaughan et al. and Zacharias et al. reported that

50 μm. **c.** Proposed lung regeneration after SARS-CoV-2 infection of hamster lung in graphic summary: During acute phase of SARS-CoV-2 infection (4&7dpi), CK14+ basal cells actively contributed to regeneration of bronchiolar epithelium. In alveolar, AT2 cells were damaged massively due to virus attack. Remaining AT2 cells self-renewed. CK14+ basal cells migrated and differentiated to AT2 cells for alveolar repair. At 14dpi, most bronchiolar and part of alveolar resumed to normal structure, while aberrant CK14+ basal cells differentiation lead to formation of foci of bronchiolization with club cells and ciliated cells, which persisted until 120dpi (the end point of observation).

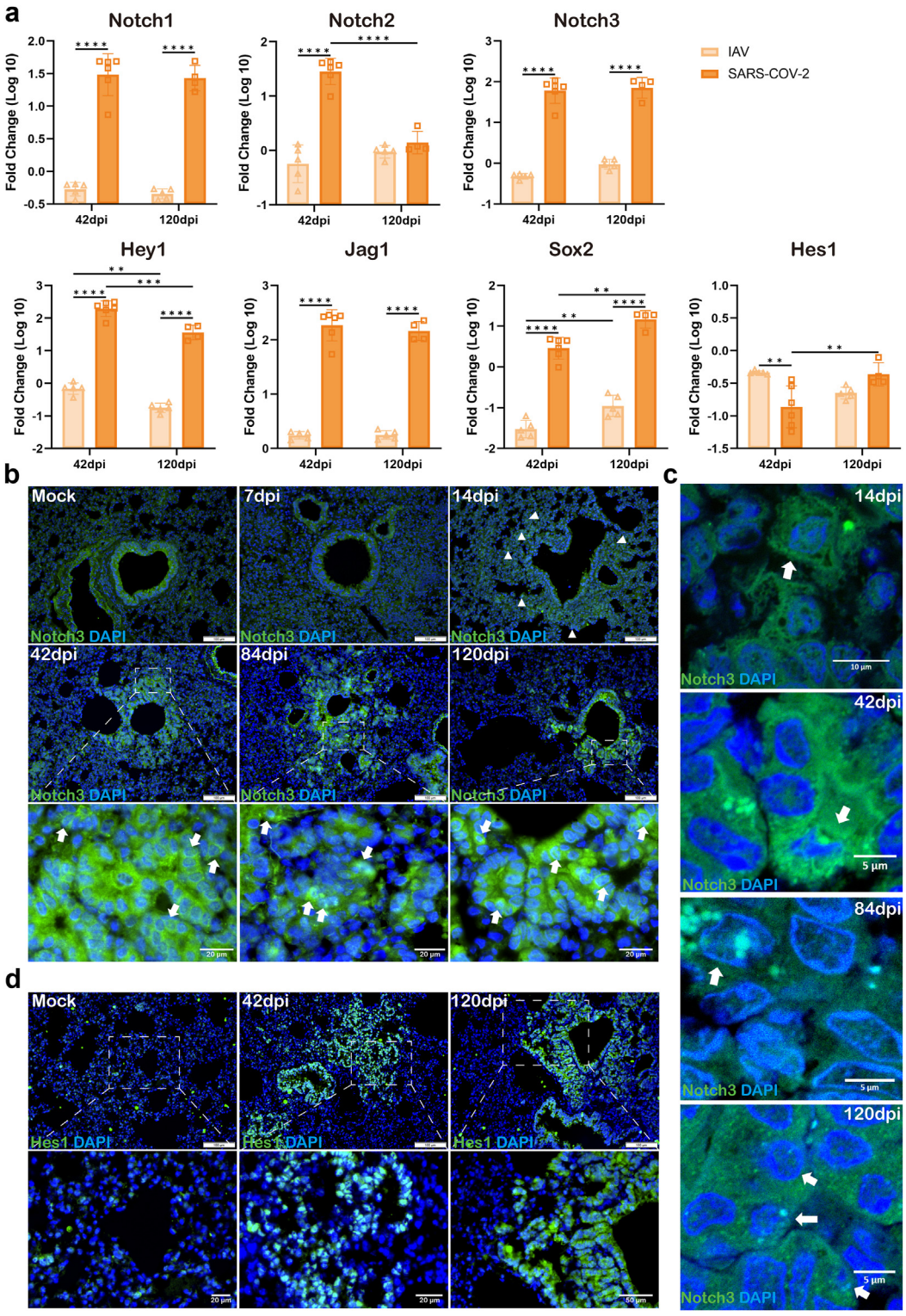

Fig. 8: **Highly elevated Notch signaling long after SARS-CoV-2 infection in hamster lung. a.** Relative mRNA expression levels of Notch signaling related genes in the lung tissues in SARS-CoV-2 and IAV infected hamsters. n = 5 for IAV 42&120dpi, 6 for SARS-CoV-2 42dpi, 4 for SARS-CoV-2 120dpi. Data represents mean ± SD. **b.** Representative images of immunofluorescence stained Notch3 (green) in mock and SARS-CoV-2 infected hamster lung at 7, 14, 42, 84 and 120dpi. Scale bar = 100 μm or 20 μm. White triangles indicate Notch3 positive cells. White

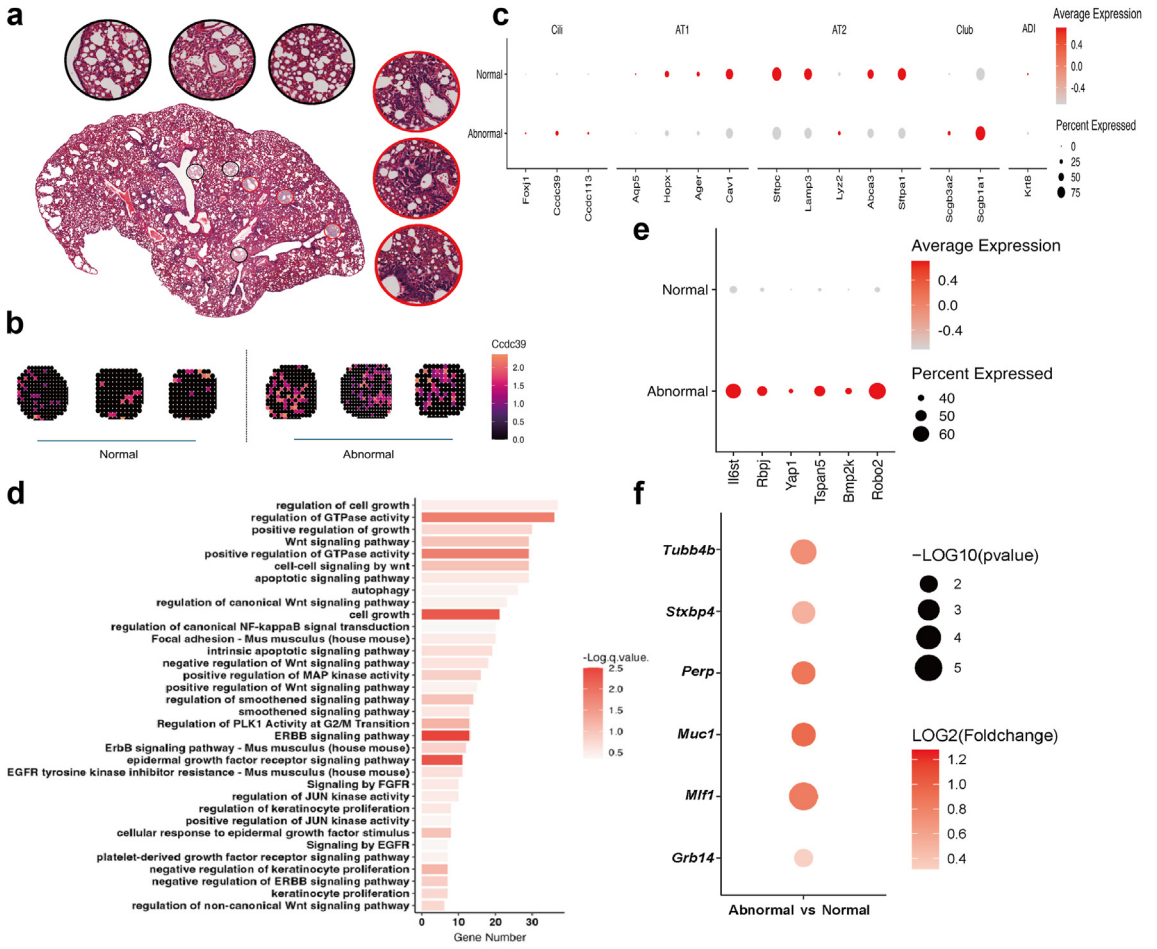

Fig. 9: **Spatial transcriptomics of SARS-CoV-2 infected hamster lung. a.** Six tissue regions representing abnormal (red circled), or normal (black circled) alveolar structures based on histological features shown in the H&E section. **b.** *Ccdc39* gene expression in selected normal (left) and abnormal (right) tissue regions. **c.** Differential expression of genes expressed on ciliated cells, AT1 cells, AT2 cells, club cells and ADI cells in selected normal and abnormal tissue regions. **d.** Enriched pathways based on the up-regulated genes in abnormal tissue regions. **e.** Differential expression of genes associated with positive regulation of Notch signaling pathway in selected normal and abnormal tissue regions. **f.** Differential expression of genes related to cancer in selected normal and abnormal tissue regions.

the level of lung injury is an important determining factor for activation of lung progenitor cells.[12,55] In mild alveoli injury, non-alveolar progenitors such as BASCs and LNEPs may not be activated. We presume this may explain, in part, our findings in A (H1N1)pdm09 infected hamster lung, while we think it is mostly attributed to SARS-CoV-2 infection induced long lasting inflammation and underlying sustained molecular events.

In addition to causing long-lasting respiratory symptoms, persistent chronic lung histological damage flag a signal for the potential risk of developing lung carcinoma. Firstly, pulmonary fibrosis is a well-accepted risk factor for lung cancer owing to the cellular and molecular pathways shared in these two conditions.[56] Secondly, alveolar-bronchiolization is considered a potential precursor lesion for lung cancer, it was previously detected in up to 12% of non-small cell lung cancer resection specimens.[57] Importantly, the existence of these histological lesions was accompanied by sustained activation of Notch, Wnt pathway and

arrows indicate Notch3 signals inside nuclei. **c.** Representative magnified images of immunofluorescence stained Notch3 (green) captured by confocal microscopy in SARS-CoV-2 infected hamster lung at 14, 42, 84 and 120dpi. Scale bar = 5 μm or 10 μm. White arrows indicate Notch3 signals inside nuclei. **d.** Representative images of immunofluorescence stained Hes1 (green) in mock and SARS-CoV-2 infected hamster lung at 42 and 120dpi. Scale bar = 100 μm, 50 μm or 20 μm. White arrows indicate Notch3 positive cells. *p < 0.05, **p < 0.01, ****p < 0.0001 by Two-way ANOVA with Tukey's multiple comparisons test (a).

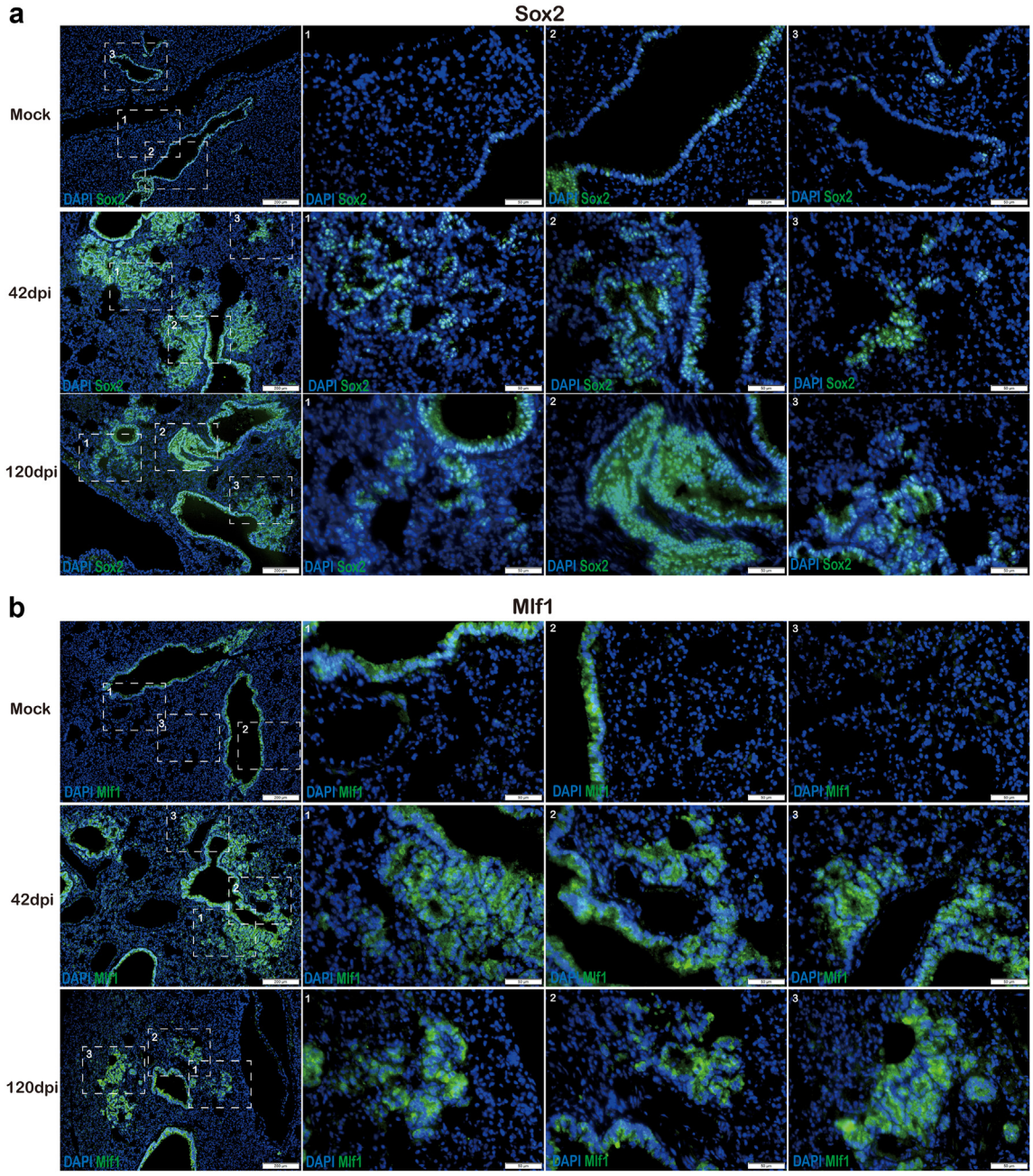

Fig. 10: **Highly expressed Sox2 and Mlf1 in cells in bronchiolization foci of SARS-CoV-2 infected hamster lung. a.** Representative images of immunofluorescence stained Sox2 (green) in mock or SARS-CoV-2 infected hamster lungs at 42 and 120dpi. Scale bar = 200 μm or 50 μm. **b.** Representative images of immunofluorescence stained Mlf1 (green) in mock or SARS-CoV-2 infected hamster lungs at 42 and 120dpi. Scale bar = 200 μm or 50 μm.

upregulation of genes related to pathways in cancer. Balanced Notch signaling is vital in cell fate determination and tumor cell initiation, proliferation, differentiation and apoptosis,[58,59] Altered Notch1 expression was reported to have oncogene function.[58,60] Our spatial transcriptomics further demonstrated some tumor related genes upregulated in the abnormal regions of lung bronchiolization foci, including *Sox2*,[61] *Stxbp4*,[62,63] *Tubb4b*,[63,64] *Mlf1*,[65] *Perp*,[66] *Muc1*[67] and *Grb14*.[68] For instance, *Stxbp4* overexpression was associated with lung cancer cell growth[62]; *Tubb4b* expression is essential for maintenance cancer stem cell niche via cooperation with Ephrin-B1. In supporting the transcriptomic changes, we then did IF staining and demonstrated

extensive signals of Hes1, Mlf1 and Sox2 in the cells of bronchiolization foci. All these suggest that the cells in the bronchiolization foci are not likely to be at quiescent state, but active. The association of these proteins with cancers was previously documented in colon cancer,[69] lung adenocarcinoma[70] for Hes1 and Mlf1, respectively; while overexpression of Sox2 promotes cancer cell proliferation, survival, invasion/metastasis.[71] At this stage, we only speculate the possibility of carcinogenesis from these tissue lesions, even so, when considering the factors like cigarette smoking, alcohol drinking, air pollution in a human's lifetime.

In summary, our study provides evidence of SARS-CoV-2 caused persistent chronic inflammation with residual viral components lingering in the lung. Diffused fibrotic lesion together with the multiple foci of alveolar-bronchiolization in the lung could be the major cause for sustained respiratory symptoms. Aberrant CK14+ basal cells activation and differentiation during lung regeneration, leads to formation of alveolar-bronchiolization which persisted in the lung potentially due to continuous Notch signaling. This study advances our understanding of the mechanism of respiratory PASC. Further investigation and continued clinical surveillance for disease progression are warranted.

There are some limitations in the current study. We have not studied the exact roles of viral positive macrophages in the development of long-term lung tissue damage, which is mainly due to the lack of adequate hamster cell makers and antibodies. This study did not cover the information on the dynamic and process of alveolar type 1 cell regeneration. Lineage-tracing of CK14+ basal cells are needed for further study. We were unable to provide direct evidence on how the Notch signaling activated CK14+ basal cell and altered its proliferation and differentiation in the process of lung regeneration. Another limitation is that our pdmH1N1 influenza infection model only induces interstitial pneumonia with less severe alveolar damage than SARS-CoV-2 infection in hamsters. The difference in disease severity at acute infection may affect, to some degree, our understanding of the long-term lung sequela. A respiratory virus infection model that causes diffuse alveolar damage would be favorable for a comparative study.

Contributors

CL, NX, WS, AH-CL, FL, JF-WC, K-YY, HC and AJ-XZ had roles in the study design, data collection, data analysis, data interpretation, and writing of the manuscript. ZY, YC, JC and AC-YL had roles in the experiments, data collection, data analysis. ZO, WS, XC and PR conducted the Stereo-seq experiment and analysis. HC had roles in data interpretation and writing of the manuscript. CL, NX and WS have accessed and verified the underlying data. All authors reviewed and approved the final version of the manuscript.

Data sharing statement

The spatial transcriptomic data and Bulk RNAseq transcriptomic data supporting this study have been deposited into CNSA (CNGB Sequence Archive) of CNGBdb (https://db.cngb.org/cnsa/) under the project number STT0000082 and CNP0005559.

Declaration of interests

We declare no competing interests.

Acknowledgements

We thank China National GeneBank for providing sequencing services and STOmics Cloud (https://cloud.stomics.tech) for their support in Stereo-seq data analysis. This study was partly supported by funding from the Collaborative Research Fund (C7060-21G) and Theme-Based Research Scheme (T11-709/21-N), the Research Grants Council of the Hong Kong Special Administrative Region; the National Natural Science Foundation of China General Program (82272337); the Health and Medical Research Fund (20190572), the Food and Health Bureau, The Government of the Hong Kong Special Administrative Region; Health@InnoHK, Innovation and Technology Commission, the Government of the Hong Kong Special Administrative Region; Partnership Programme of Enhancing Laboratory Surveillance and Investigation of Emerging Infectious Diseases and Antimicrobial Resistance for the Department of Health of the Hong Kong Special Administrative Region Government; Sanming Project of Medicine in Shenzhen, China (SZSM201911014); the High Level-Hospital Program, Health Commission of Guangdong Province, China; National Key Research and Development Program of China(projects 2021YFC0866100 and 2023YFC3041600); Emergency Collaborative Project of Guangzhou Laboratory (EKPG22-01); the Major Science and Technology Program of Hainan Province (ZDKJ202003); the research project of Hainan Academician Innovation Platform (YSPTZX202004); the University of Hong Kong Outstanding Young Researcher Award; and the University of Hong Kong Research Output Prize (Li Ka Shing Faculty of Medicine); and donations from May Tam Mak Mei Yin, Richard Yu and Carol Yu, the Shaw Foundation Hong Kong, Michael Seak-Kan Tong, Lee Wan Keung Charity Foundation Limited, Providence Foundation Limited (in memory of the late Lui Hac-Minh), Hong Kong Sanatorium and Hospital, Hui Ming, Hui Hoy and Chow Sin Lan Charity Fund Limited, The Chen Wai Wai Vivien Foundation Limited, Chan Yin Chuen Memorial Charitable Foundation, Marina Man-Wai Lee, the Hong Kong Hainan Commercial Association South China Microbiology Research Fund, Perfect Shape Medical Limited, Kai Chong Tong, Tse Kam Ming Laurence, Foo Oi Foundation Limited, Betty Hing-Chu Lee, Ping Cham So, and Lo Ying Shek Chi Wai Foundation.

Appendix A. Supplementary data

Supplementary data related to this article can be found at https://doi.org/10.1016/j.ebiom.2024.105363.

References

1 World Health Organization. *WHO Coronavirus (COVID-19) dashboard*. 2024. Accessed on May 09, 2024.
2 Davis HE, McCorkell L, Vogel JM, Topol EJ. Long COVID: major findings, mechanisms and recommendations. *Nat Rev Microbiol*. 2023;21(3):133–146.
3 Ballering AV, van Zon SKR, Olde Hartman TC, Rosmalen JGM. Persistence of somatic symptoms after COVID-19 in The Netherlands: an observational cohort study. *Lancet*. 2022;400(10350):452–461.
4 Stewart I, Jacob J, George PM, et al. Residual lung abnormalities after COVID-19 hospitalization: interim analysis of the UKILD post-COVID-19 study. *Am J Respir Crit Care Med*. 2023;207(6):693–703.
5 Adegunsoye A, Baccile R, Best TJ, et al. Pharmacotherapy and pulmonary fibrosis risk after SARS-CoV-2 infection: a prospective nationwide cohort study in the United States. *Lancet Reg Health Am*. 2023;25:100566.
6 Laura F, Samuel M, Fasihul AK, et al. Parenchymal lung abnormalities following hospitalisation for COVID-19 and viral pneumonitis: a systematic review and meta-analysis. *Thorax*. 2023;78(2):191.
7 Sherif ZA, Gomez CR, Connors TJ, Henrich TJ, Reeves WB, Force RMPT. Pathogenic mechanisms of post-acute sequelae of SARS-CoV-2 infection (PASC). *Elife*. 2023;12:e86002.

8 Heydemann L, Ciurkiewicz M, Beythien G, et al. Hamster model for post-COVID-19 alveolar regeneration offers an opportunity to understand post-acute sequelae of SARS-CoV-2. *Nat Commun*. 2023;14(1):3267.
9 Chen J, Wu H, Yu Y, Tang N. Pulmonary alveolar regeneration in adult COVID-19 patients. *Cell Res*. 2020;30(8):708–710.
10 Kotton DN, Morrisey EE. Lung regeneration: mechanisms, applications and emerging stem cell populations. *Nat Med*. 2014;20(8):822–832.
11 Olajuyin AM, Zhang X, Ji H-L. Alveolar type 2 progenitor cells for lung injury repair. *Cell Death Discov*. 2019;5(1):63.
12 Vaughan AE, Brumwell AN, Xi Y, et al. Lineage-negative progenitors mobilize to regenerate lung epithelium after major injury. *Nature*. 2015;517(7536):621–625.
13 Salahudeen AA, Choi SS, Rustagi A, et al. Progenitor identification and SARS-CoV-2 infection in human distal lung organoids. *Nature*. 2020;588(7839):670–675.
14 Pardo-Saganta A, Law BM, Tata PR, et al. Injury induces direct lineage segregation of functionally distinct airway basal stem/progenitor cell subpopulations. *Cell Stem Cell*. 2015;16(2):184–197.
15 Wu M, Zhang X, Lin Y, Zeng Y. Roles of airway basal stem cells in lung homeostasis and regenerative medicine. *Respir Res*. 2022;23(1):122.
16 Schreiner T, Allnoch L, Beythien G, et al. SARS-CoV-2 infection dysregulates cilia and basal cell homeostasis in the respiratory epithelium of hamsters. *Int J Mol Sci*. 2022;23(9):5124.
17 Carraro G, Mulay A, Yao C, et al. Single-cell reconstruction of human basal cell diversity in normal and idiopathic pulmonary fibrosis lungs. *Am J Respir Crit Care Med*. 2020;202(11):1540–1550.
18 Sano E, Suzuki T, Hashimoto R, et al. Cell response analysis in SARS-CoV-2 infected bronchial organoids. *Commun Biol*. 2022;5(1):516.
19 Wang C, Khatun MS, Zhang Z, et al. COVID-19 and influenza infections mediate distinct pulmonary cellular and transcriptomic changes. *Commun Biol*. 2023;6(1):1265.
20 Hynds RE, Janes SM. Airway basal cell heterogeneity and lung squamous cell carcinoma. *Cancer Prev Res*. 2017;10(9):491–493.
21 Shaykhiev R. Airway basal cells in chronic obstructive pulmonary disease: a continuum or a dead end? *Am J Respir Cell Mol Biol*. 2021;65(1):10–12.
22 Chan JF, Zhang AJ, Yuan S, et al. Simulation of the clinical and pathological manifestations of coronavirus disease 2019 (COVID-19) in a golden Syrian hamster model: implications for disease pathogenesis and transmissibility. *Clin Infect Dis*. 2020;71(9):2428–2446.
23 Muñoz-Fontela C, Dowling WE, Funnell SGP, et al. Animal models for COVID-19. *Nature*. 2020;586(7830):509–515.
24 Sia SF, Yan L-M, Chin AWH, et al. Pathogenesis and transmission of SARS-CoV-2 in golden hamsters. *Nature*. 2020;583(7818):834–838.
25 Zhang AJ, Lee AC, Chan JF, et al. Coinfection by severe acute respiratory syndrome coronavirus 2 and influenza A(H1N1)pdm09 virus enhances the severity of pneumonia in golden Syrian hamsters. *Clin Infect Dis*. 2021;72(12):e978–e992.
26 Zheng B, Chan KH, Zhang AJ, et al. D225G mutation in hemagglutinin of pandemic influenza H1N1 (2009) virus enhances virulence in mice. *Exp Biol Med*. 2010;235(8):981–988.
27 Charan J, Kantharia ND. How to calculate sample size in animal studies? *J Pharmacol Pharmacother*. 2013;4(4):303–306.
28 Dinnon KH 3rd, Leist SR, Okuda K, et al. SARS-CoV-2 infection produces chronic pulmonary epithelial and immune cell dysfunction with fibrosis in mice. *Sci Transl Med*. 2022;14(664):eabo5070.
29 Hübner RH, Gitter W, El Mokhtari NE, et al. Standardized quantification of pulmonary fibrosis in histological samples. *Biotechniques*. 2008;44(4):507–511, 14-511.
30 Kim D, Paggi JM, Park C, Bennett C, Salzberg SL. Graph-based genome alignment and genotyping with HISAT2 and HISAT-genotype. *Nat Biotechnol*. 2019;37(8):907–915.
31 Love MI, Huber W, Anders S. Moderated estimation of fold change and dispersion for RNA-seq data with DESeq2. *Genome Biol*. 2014;15(12):550.
32 Zhou Y, Zhou B, Pache L, et al. Metascape provides a biologist-oriented resource for the analysis of systems-level datasets. *Nat Commun*. 2019;10(1):1523.
33 Chen A, Liao S, Cheng M, et al. Spatiotemporal transcriptomic atlas of mouse organogenesis using DNA nanoball-patterned arrays. *Cell*. 2022;185(10):1777–1792.e21.
34 La Manno G, Soldatov R, Zeisel A, et al. RNA velocity of single cells. *Nature*. 2018;560(7719):494–498.
35 Hao Y, Hao S, Andersen-Nissen E, et al. Integrated analysis of multimodal single-cell data. *Cell*. 2021;184(13):3573–3587.e29.
36 Fernandez IE, Eickelberg O. The impact of TGF-β on lung fibrosis: from targeting to biomarkers. *Proc Am Thorac Soc*. 2012;9(3):111–116.
37 McKeown S, Richter AG, Kane O, McAuley DF, Thickett DR. MMP expression and abnormal lung permeability are important determinants of outcome in IPF. *Eur Respir J*. 2009;33(1):77.
38 Yuan S, Ye ZW, Liang R, et al. Pathogenicity, transmissibility, and fitness of SARS-CoV-2 omicron in Syrian hamsters. *Science*. 2022;377(6604):428–433.
39 Merveille AC, Davis EE, Becker-Heck A, et al. CCDC39 is required for assembly of inner dynein arms and the dynein regulatory complex and for normal ciliary motility in humans and dogs. *Nat Genet*. 2011;43(1):72–78.
40 Lee AC, Zhang AJ, Chan JF, et al. Oral SARS-CoV-2 inoculation establishes subclinical respiratory infection with virus shedding in golden Syrian hamsters. *Cell Rep Med*. 2020;1(7):100121.
41 Proal AD, VanElzakker MB, Aleman S, et al. SARS-CoV-2 reservoir in post-acute sequelae of COVID-19 (PASC). *Nat Immunol*. 2023;24(10):1616–1627.
42 Merad M, Martin JC. Pathological inflammation in patients with COVID-19: a key role for monocytes and macrophages. *Nat Rev Immunol*. 2020;20(6):355–362.
43 Zeqing F, Bo D, Rongshuai W, et al. The novel severe acute respiratory syndrome coronavirus 2 (SARS-CoV-2) directly decimates human spleens and lymph nodes. *medRxiv*. 2020. https://doi.org/10.1101/2020.03.27.20045427.
44 Huot N, Planchais C, Rosenbaum P, et al. SARS-CoV-2 viral persistence in lung alveolar macrophages is controlled by IFN-γ and NK cells. *Nat Immunol*. 2023;24(12):2068–2079.
45 Kee J, Thudium S, Renner DM, et al. SARS-CoV-2 disrupts host epigenetic regulation via histone mimicry. *Nature*. 2022;610(7931):381–388.
46 Mandal S, Barnett J, Brill SE, et al. 'Long-COVID': a cross-sectional study of persisting symptoms, biomarker and imaging abnormalities following hospitalisation for COVID-19. *Thorax*. 2021;76(4):396–398.
47 Bazdyrev E, Rusina P, Panova M, Novikov F, Grishagin I, Nebolsin V. Lung fibrosis after COVID-19: treatment prospects. *Pharmaceuticals*. 2021;14(8):807.
48 Frere JJ, Serafini RA, Pryce KD, et al. SARS-CoV-2 infection in hamsters and humans results in lasting and unique systemic perturbations after recovery. *Sci Transl Med*. 2022;14(664):eabq3059.
49 Hansen F, Meade-White K, Clancy C, et al. SARS-CoV-2 reinfection prevents acute respiratory disease in Syrian hamsters but not replication in the upper respiratory tract. *Cell Rep*. 2022;38(11):110515.
50 Ray S, Chiba N, Yao C, et al. Rare SOX2(+) airway progenitor cells generate KRT5(+) cells that repopulate damaged alveolar parenchyma following influenza virus infection. *Stem Cell Rep*. 2016;7(5):817–825.
51 Xing Y, Li A, Borok Z, Li C, Minoo P. NOTCH1 is required for regeneration of Clara cells during repair of airway injury. *Stem Cells*. 2012;30(5):946–955.
52 Mori M, Mahoney JE, Stupnikov MR, et al. Notch3-Jagged signaling controls the pool of undifferentiated airway progenitors. *Development*. 2015;142(2):258–267.
53 Eenjes E, Buscop-van Kempen M, Boerema-de Munck A, et al. SOX21 modulates SOX2-initiated differentiation of epithelial cells in the extrapulmonary airways. *Elife*. 2021;10:e57325.
54 Rosa BA, Ahmed M, Singh DK, et al. IFN signaling and neutrophil degranulation transcriptional signatures are induced during SARS-CoV-2 infection. *Commun Biol*. 2021;4(1):290.
55 Zacharias WJ, Frank DB, Zepp JA, et al. Regeneration of the lung alveolus by an evolutionarily conserved epithelial progenitor. *Nature*. 2018;555(7695):251–255.
56 Ballester B, Milara J, Cortijo J. Idiopathic pulmonary fibrosis and lung cancer: mechanisms and molecular targets. *Int J Mol Sci*. 2019;20(3):593.
57 Wang X-Y, Demelash A, Kim H, et al. Matrilysin-1 mediates bronchiolization of alveoli, a potential premalignant change in lung cancer. *Am J Pathol*. 2009;175(2):592–604.
58 Zou B, Zhou XL, Lai SQ, Liu JC. Notch signaling and non-small cell lung cancer. *Oncol Lett*. 2018;15(3):3415–3421.

59 Zhang H, Yang Y, Li X, Yuan X, Chu Q. Targeting the Notch signaling pathway and the Notch ligand, DLL3, in small cell lung cancer. *Biomed Pharmacother*. 2023;159:114248.
60 Maraver A, Fernández-Marcos PJ, Herranz D, et al. Therapeutic effect of γ-secretase inhibition in KrasG12V-driven non-small cell lung carcinoma by derepression of DUSP1 and inhibition of ERK. *Cancer Cell*. 2012;22(2):222–234.
61 Correia LL, Johnson JA, McErlean P, et al. SOX2 drives bronchial dysplasia in a novel organotypic model of early human squamous lung cancer. *Am J Respir Crit Care Med*. 2017;195(11):1494–1508.
62 Otaka Y, Rokudai S, Kaira K, et al. STXBP4 drives tumor growth and is associated with poor prognosis through PDGF receptor signaling in lung squamous cell carcinoma. *Clin Cancer Res*. 2017;23(13):3442–3452.
63 Dharmapal D, Jyothy A, Mohan A, et al. β-Tubulin isotype, TUBB4B, regulates the maintenance of cancer stem cells. *Front Oncol*. 2021;11:788024.
64 Amin A, Koul AM, Wani UM, et al. Dissection of paracrine/autocrine interplay in lung tumor microenvironment mimicking cancer cell-monocyte co-culture models reveals proteins that promote inflammation and metastasis. *BMC Cancer*. 2023;23(1):926.
65 Li Z, Yang Y, Wu K, Li Y, Shi M. Myeloid leukemia factor 1: a "double-edged sword" in health and disease. *Front Oncol*. 2023;13:1124978.
66 Liu Z, Han S, Luo Y, et al. PERP may affect the prognosis of lung adenocarcinoma by inhibiting apoptosis. *Cancer Manag Res*. 2024;16:199–214.
67 Saltos A, Khalil F, Smith M, et al. Clinical associations of mucin 1 in human lung cancer and precancerous lesions. *Oncotarget*. 2018;9(86):35666–35675.
68 Chen Q, Liu Z, Zhong L, et al. High expression of growth factor receptor-bound protein 14 predicts clinical progression and poor prognosis in patients with lung adenocarcinoma. *Res Square*. 2020. https://doi.org/10.21203/rs.3.rs-58001/v1.
69 Gao F, Zhang Y, Wang S, et al. Hes1 is involved in the self-renewal and tumourigenicity of stem-like cancer cells in colon cancer. *Sci Rep*. 2014;4:3963.
70 Li X, Min S, Wang H, et al. MLF1 protein is a potential therapy target for lung adenocarcinoma. *Int J Clin Exp Pathol*. 2018;11(7):3533–3541.
71 Zhang S, Xiong X, Sun Y. Functional characterization of SOX2 as an anticancer target. *Signal Transduct Targeted Ther*. 2020;5(1):135.